This is a repository copy of *Absolute quantification of cellular levels of photosynthesis-related proteins in Synechocystis sp. PCC 6803*.

White Rose Research Online URL for this paper:
https://eprints.whiterose.ac.uk/194910/

Version: Published Version

Article:

ORIGINAL ARTICLE

Absolute quantification of cellular levels of photosynthesis-related proteins in *Synechocystis* sp. PCC 6803

Philip J. Jackson[1,2] · Andrew Hitchcock[1] · Amanda A. Brindley[1] · Mark J. Dickman[2] · C. Neil Hunter[1]

Abstract

Quantifying cellular components is a basic and important step for understanding how a cell works, how it responds to environmental changes, and for re-engineering cells to produce valuable metabolites and increased biomass. We quantified proteins in the model cyanobacterium *Synechocystis* sp. PCC 6803 given the general importance of cyanobacteria for global photosynthesis, for synthetic biology and biotechnology research, and their ancestral relationship to the chloroplasts of plants. Four mass spectrometry methods were used to quantify cellular components involved in the biosynthesis of chlorophyll, carotenoid and bilin pigments, membrane assembly, the light reactions of photosynthesis, fixation of carbon dioxide and nitrogen, and hydrogen and sulfur metabolism. Components of biosynthetic pathways, such as those for chlorophyll or for photosystem II assembly, range between 1000 and 10,000 copies per cell, but can be tenfold higher for CO_2 fixation enzymes. The most abundant subunits are those for photosystem I, with around 100,000 copies per cell, approximately 2 to fivefold higher than for photosystem II and ATP synthase, and 5–20 fold more than for the cytochrome b_6f complex. Disparities between numbers of pathway enzymes, between components of electron transfer chains, and between subunits within complexes indicate possible control points for biosynthetic processes, bioenergetic reactions and for the assembly of multisubunit complexes.

Keywords *Synechocystis* · Cyanobacteria · Mass spectrometry · Photosynthesis · Photosystem · Assembly factor · Chlorophyll · Electron transport

Introduction

Cyanobacteria evolved approximately 2.4 billion years ago as the only prokaryotes that utilize solar energy to oxidize water. Electron transport coupled to proton translocation then drives the production of the ATP and NADPH needed for CO_2 fixation and other metabolic processes and reviewed by Lea-Smith et al. (2016). Cyanobacteria have colonized almost every terrestrial and aquatic habitat, with marine species alone responsible for an estimated carbon capture rate of 4×10^{12} kg y^{-1} (Rousseaux and Gregg 2014), contributing 3.8% of global net primary production (Field et al. 1998). In view of their ecological significance, the effects of the anthropogenic increase in atmospheric CO_2 on cyanobacterial populations and their influence on the entire biosphere are important areas of study (Ullah et al. 2018).

Some avenues of research are specific for cyanobacteria, but others have wider relevance to photosynthesis in algae and plants due to the common ancestry of cyanobacteria and chloroplasts (Yoon et al. 2004). Similarities between cyanobacterial and eukaryotic photosystems have led to the adoption of several species of cyanobacteria, often thermophiles, as models for exploring the fundamental mechanisms that underpin oxygenic photosynthesis (Ferreira et al. 2004; Umena et al. 2011; Suga et al. 2015; Gisriel et al. 2019; Çoruh et al. 2021). The early availability of a complete genome sequence for *Synechocystis* sp. PCC 6803 (hereafter *Synechocystis*) was also an invaluable resource for studies of photosynthesis and many other cellular functions. This was the first such information for any phototroph, and only the third genome sequence for any organism (Kaneko et al. 1996). This advance, as well as the amenability of this cyanobacterium to genetic manipulation (Vermaas 1994), hastened the adoption of *Synechocystis* as a model for photosynthesis research. One recent example, which builds upon the evolutionary relationship between

✉ Philip J. Jackson
p.j.jackson@sheffield.ac.uk

1 Plants, Photosynthesis and Soil, School of Biosciences, University of Sheffield, Sheffield S10 2TN, UK

2 Department of Chemical and Biological Engineering, University of Sheffield, Sheffield S1 3JD, UK

chloroplasts and cyanobacteria, is the use of *Synechocystis* as a platform for the rapid development of genetic diversity by adaptive evolution. Laboratory-evolved mutations in cyanobacteria such as *Synechocystis* that confer enhanced efficiency for converting solar energy into biomass may then be transferable to crop plants with the aim of increasing yield (Leister 2012; Dann and Leister 2017; Dann et al. 2021). Model cyanobacterial species have also been valuable for designing solar-powered systems for synthetic biology (reviewed by Sengupta et al. 2018).

In view of its universally recognized importance in photosynthesis research, *Synechocystis* has been a frequent target for mass spectrometry (MS)-based proteomic analysis, as reviewed by Gao et al. (2015) and Battchikova et al. (2018). A principal focus has been on the comparative quantification of protein abundance following adaptation to varying culture conditions (for example see Fulda et al. 2000; Hong et al. 2014; Angeleri et al. 2019) and mutant strains have been used as tools for the dissection of adaptive and regulatory pathways (for example see Tokumaru et al. 2018; Krynická et al. 2019). This approach has also mapped proteins to their subcellular locations to track the development of thylakoid membranes (TMs), the specialized photosynthetic membranes that cyanobacteria, algae and plants all have in common (Kwon et al. 2010; Pisareva et al. 2011). More recently, a proteomic catalog of subcellular localization has been produced, comprising 1712 proteins (Baers et al. 2019).

Photosynthesis research is starting to encompass larger and larger structures, from complexes, to supercomplexes, to membrane organization studied by atomic force microscopy and finally to whole cells (MacGregor-Chatwin et al. 2017; Casella et al. 2017; Zhao et al. 2020). Here, spectacular recent advances in cryo-electron tomography, augmented by super-resolution fluorescence imaging, are starting to reveal the molecular details of cyanobacterial cells, their internal cellular components and their membrane architectures (Rast et al. 2019; Huokko et al. 2021). With this focus on cells it is appropriate to count cellular components in terms of the copy numbers of proteins per cell, which would appear to be a basic requirement for understanding cellular function, and for manipulations of cells and their pathways for synthetic biology purposes. Yet despite the considerable volume of proteomic information now available for *Synechocystis* and other cyanobacteria, to our knowledge there has been no MS-based absolute quantification of proteins in terms of copy number per cell (cpc). So far, cpc determination has been confined to photosystems I and II (PSI and PSII) using absorption spectra associated with their bound chlorophylls (Fujita and Murakami 1987; Hihara et al. 1998; Keren et al. 2004; Fraser et al. 2013; MacGregor-Chatwin et al. 2017). MS-derived absolute quantitative studies of proteins are nevertheless commonplace, having been undertaken in many different organisms and subcellular systems. Some examples, employing both stable isotope labelled (SIL) standards and label-free approaches, are: *Escherichia coli* (Wiśniewskia and Rakus 2014), *Leptospira interrogans* (Malmström et al. 2009), chromatophores in *Rhodobacter sphaeroides* (Cartron et al. 2014), glycolytic pathway enzymes in *Saccharomyces cerevisiae* (Carroll et al. 2011) and xenobiotic metabolizing enzymes in human liver microsomes (Li et al. 2015). Two of the SIL-based methods are confined to the absolute quantification of single or low numbers of proteins and involve calibration with either ^{15}N-labelled synthetic peptide fragments (usually tryptic) mapping to the target protein(s) (Kirkpatrick et al. 2005) or full-length SIL proteins produced in *E. coli* grown in ^{15}N-containing liquid culture (Brun et al. 2007; Singh et al. 2009). For larger scale absolute quantification the high-financial cost of the former and long lead-time of the latter are potential obstacles that make label-free quantification (LFQ) methods more attractive and therefore more widely used. Since no single LFQ method has emerged as the 'gold standard', numerous performance comparisons can be found in the literature (for example see Arike et al. 2013; Fabre et al. 2014; Krey et al. 2014; Al Shweiki et al. 2017; Tang et al. 2019).

Here, we employed a third SIL-based quantification method that is more feasible for this larger scale study than the two options described above. It is also well characterized and uses artificial ^{15}N-labelled proteins comprising concatenated tryptic peptides mapping to the target proteins (Pratt et al. 2006; Brownridge et al. 2013). To provide further validation and extend the range of target proteins, we additionally employed three LFQ methods: (1) iBAQ (intensity-based absolute quantification) (Schwanhäusser et al. 2011) based on data-dependent acquisition (DDA) and Top3 (Silva et al. 2006), based on both (2) DDA and (3) data-independent acquisition (DIA) (Venable et al. 2004). We demonstrate that our MS-based absolute quantification of PSI and PSII complexes is in close agreement with copy numbers determined spectrophotometrically, both here and in earlier studies (Fujita and Murakami 1987; Hihara et al. 1998; Keren et al. 2004; Fraser et al. 2013; MacGregor-Chatwin et al. 2017). Similarly, we show subunit stoichiometry in the ATP synthase complex aligns with the known structure for the complex in bacteria (Guo et al. 2019). Having validated our approach, we present the first report of MS-based absolute quantification of cytochrome b_6f (cytb_6f) subunits, associated mediators of electron transport and downstream electron-accepting metabolic processes including CO_2 fixation. Also quantified are enzymes and auxiliary proteins in the chlorophyll (Chl), carotenoid and phycobilin biosynthesis pathways, together with assembly factors implicated in TM biogenesis and PSI and PSII assembly. These 97 proteins and their interrelationships are summarized in Figs. 1, 2, 3, 4,

5. Finally, we exploit our quantitative analyses to present the cellular abundances of 1081 proteins in *Synechocystis*.

Materials and methods

Cell culture

Synechocystis sp. PCC 6803 cells (wild-type substrain GT-P, Tichý et al. 2016) were grown under photoautotrophic conditions in a rotary shaking incubator at 150 rpm under moderate light conditions (30 μmol photons $m^{-2} s^{-1}$) at 30 °C in liquid BG11 medium (Rippka et al. 1979) supplemented with 10 mM TES-KOH ($pH = 8.2$). Three replicate 80 mL cultures were harvested at $OD_{750} = 0.6$–0.7 by centrifugation at 5000 xg for 20 min at 4 °C. Cells were counted in a hemocytometer after allowing them to settle on the slide for 30 min and stored as pellets at -80 °C after flash-freezing in liquid nitrogen.

Preparation of artificial stable isotope-labelled internal standards

Six artificial SIL internal standard proteins comprising concatenated proteotypic tryptic peptide sequences mapping to thirty-seven target proteins were designed as described previously (Pratt et al. 2006; Brownridge et al. 2013) These proteins were expressed in *E. coli* in M9 medium containing $(^{15}NH_4)_2SO_4$ as the sole nitrogen source and purified according to Qian et al. (2013).

Extraction and digestion of *Synechocystis* proteins for quantification

Cells (5.6×10^8) were solubilized in 100 μL 2% (w/v) sodium dodecylsulfate, 60 mM DL-dithiothreitol by vortexing with 100 μL 0.1 mm silica-zirconia beads according to Krynická et al. (2019). Three samples each corresponding to 1.6×10^8 cells were taken from each of the three replicate lysates and one set of samples was spiked with 15 pmol of each SIL standard protein. Proteins were extracted from all samples then reduced, S-alkylated and digested with pre-mixed trypsin/endoproteinase Lys-C as described by Krynická et al. (2019).

Analysis by mass spectrometry

Peptides were re-dissolved in 0.1% (v/v) trifluoroacetic acid, 3% (v/v) acetonitrile (LC grade). The samples containing SIL standards were analysed by nano-flow liquid chromatography (3 h gradient) coupled to a mass spectrometer (MS, Q Exactive HF, Thermo Scientific) at 400 ng/injection (three technical repeats of each biological replicate in randomized order). DDA parameters were as specified by Flannery et al. (2021). The remaining two sample sets for LFQ were spiked with a tryptic digest of Universal Protein Standard 2 (UPS2, Sigma-Aldrich), prepared according to the manufacturer's instructions, so that each 400 ng *Synechocystis* peptide injection was supplemented with 42.4 ng of UPS2 peptides comprising 200 fmol of the highest concentration UPS2 proteins. One of the UPS2 containing sample sets was analysed in triplicate (randomized order) by DDA as above, the other was analysed in triplicate (randomized order) by DIA using the 'DIA60' parameters described by Cole et al. (2019).

Data processing

The SIL raw MS data-files were first converted to Mascot Generic Format (MGF) using the MSConvert tool in ProteoWizard v. 3.0.8934 (Chambers et al. 2012). The MGF files were used as input for database searching by Mascot Daemon v. 2.5.1 running with Mascot Server v. 2.5.1 (Matrix Science) against the *Synechocystis* sp. PCC 6803 Cyanobase proteome database (http://genome.kazusa.or.jp/cyanobase/Synechocystis; latest release 2003, 3672 entries). Search parameters were: enzyme, trypsin; fixed modification, carbamidomethyl (C); variable modification, oxidation (M); maximum missed cleavages, 1; mass tolerances (peptide and fragment), 0.05 Da; quantification, ^{15}N metabolic. The search results, in the form of Mascot DAT files were imported into Skyline v. 4.1.0.18169 (MacClean et al. 2010) to generate a spectral library for protein quantification by comparison between the ion intensities of tryptic peptides from *Synechocystis* cells and their ^{15}N-labelled counterparts from the internal standards. The peptide peak assignments and ^{14}N:^{15}N ratio calculations displayed by Skyline were curated manually.

The LFQ-DDA raw MS data-files were processed with MaxQuant v. 1.5.3.30 (Cox and Mann 2008) using the default parameters, with the exceptions that the match between runs and iBAQ (validated by Schwanhäusser et al. 2011) options were enabled. In addition to the *Synechocystis* database mentioned above, the search included a database of the proteins in the UPS2 standard. Identification and quantification results generated by MaxQuant were manipulated in Perseus v. 1.5.3.2 (Tyanova et al. 2016). Quantification of the target proteins was by interpolation of $\log_{10}$-transformed iBAQ intensities within regression lines calculated for the UPS2 standard proteins. The LFQ-DDA data set was also used to manually extract quantitative information based on the summed intensities of the three highest intensity tryptic peptides for each target protein, a method referred to as 'Top3' (Silva et al. 2006). Calibration was by comparison with 'Top3' intensities for the UPS2 standard proteins, as above. The LFQ-DIA raw MS data-files were

processed in Skyline with the spectral library created from an imported MaxQuant msms.txt file derived from processing LFQ-DDA MS data, with UPS2 calibration as above. The peptide peak assignments displayed by Skyline were curated manually.

Chlorophyll *a* determination

Synechocystis cells (1.2×10^8, counted as detailed above) were pelleted in a microcentrifuge at 5000 x*g* for 5 min from 1 mL of culture medium ($OD_{750} = 0.65$) and extracted with 1 mL of 100% methanol. Chl *a* was quantified by spectrophotometry according to Porra et al. (1989).

Results and discussion

Validation of protein identification and quantification

Validation of the cell counting, protein identification and absolute quantification methods are described in Supplementary Information.

Conversion of solar to chemical energy

Photosystem II

PSII is a multi-subunit complex that is integrated into the TM and contains Chl cofactors that enable its photochemical function (Ferreira et al. 2004). The process of oxygenic photosynthesis in *Synechocystis* (reviewed by Lea-Smith et al. 2016) is initiated when solar energy captured by phycobilisomes is transferred to PSII to drive the abstraction of electrons from water, producing O_2 and releasing protons into the thylakoid lumen.

The four core PSII subunits were quantified: PsbA-D, also referred to as D1, CP47, CP43 and D2 respectively, alongside one of the small subunits, PsbH. Figure 1a shows that the reaction center heterodimer subunits D1 and D2 are closely aligned at 24,000–44,000 cpc, indicated by the two horizontal dashed lines. This range is not only consistent with structural studies establishing the 1:1 stoichiometry of D1 and D2 (Umena et al. 2011; Suga et al. 2015; Gisriel et al. 2022) but also a functional assay of PSII abundance, using flash-induced O_2 yield in the related *Synechocystis* sp. PCC 6714 (Fujita and Murakami 1987), at 18,000–22,000 cpc. At the lower extent of their abundance range, CP47 and CP43 are within 24,000–44,000 cpc, however at the upper extent these subunits occur at approximately 100,000 cpc,

substantially in excess of the one subunit per complex stoichiometry in PSII (Umena et al. 2011; Suga et al. 2015; Gisriel et al. 2022). This observation may be explained by evidence for an excess of the CP47m and CP43m assembly modules over D1- and D2-containing intermediates (Tichý et al. 2016; Bečková et al. 2022), all of which would be included in our whole cell analysis. We therefore suggest that the cellular level of functional PSII complexes in *Synechocystis*, grown under the conditions employed here, is 24,000–44,000 cpc.

Like CP47 and CP43, the 7 kDa subunit PsbH is shown to occur markedly in excess of D1 and D2, at 155,500–187,000 cpc (Fig. 1a). Since PsbH has a stabilizing function, as an obligatory component of both complete, active PSII (Komenda et al. 2002) and several of its assembly intermediates (Komenda 2005), this high level would be expected.

Cytochrome b_6f complex and plastocyanin

The cytb_6f complex provides the link in the electron transport pathway between PSII and PSI in oxygenic photosynthesis and, like the photosystems, is integral to the TMs (Lea-Smith et al. 2016). In oxygenic phototrophs, this complex comprises four major and four minor subunits (reviewed by Malone et al. 2021). The four major subunits, PetA, PetB, PetC and PetD (cyt *f*, cyt b_6, the Rieske Fe-S protein (ISP) and Subunit IV (subIV) respectively) were quantified at 3500–6250, 14,000–20,000, 19,000–28,000 and 2700–8450 cpc, respectively (Fig. 1b). Despite the known stoichiometry of 1:1:1:1 in the cyanobacterial and plant cytb_6f structures (Malone et al. 2021), these ranges unexpectedly fell into lower (cyt b_6 and subIV) and higher (cyt *f* and ISP) groups. The lower end of the cpc range for subIV aligns with the 2700 cpc determined in *Thermosynechococcus elongatus* (hereafter *T. elongatus*) by Rexroth et al. (2014) who also reported an abundance of 2500 cpc for ISP, in agreement with the known stoichiometry within the complex. However, the PSII:cytb_6f ratio of 1.08–1.14 reported by Fujita and Murakami (1987) alongside our determination of PSII at 24,000–44,000 cpc suggests that, in *Synechocystis*, cytb_6f may actually align with the higher abundance cytb_6 and ISP at 14,000–28,000 cpc.

The ISP identified in this analysis was the principal PetC1 isoform encoded by the sll1316 gene. The alternative isoform (PetC2, slr1185-encoded) which is produced under low oxygen (Summerfield et. al 2008) or high light stress (Tsunoyama et al. 2009) was undetectable. The third ISP, PetC3 (sll1182-encoded) was identified in our analyses (Supplementary Data Sets S1 and S2), however, it is localized to the cytoplasmic, not thylakoid membrane (Aldridge et al.
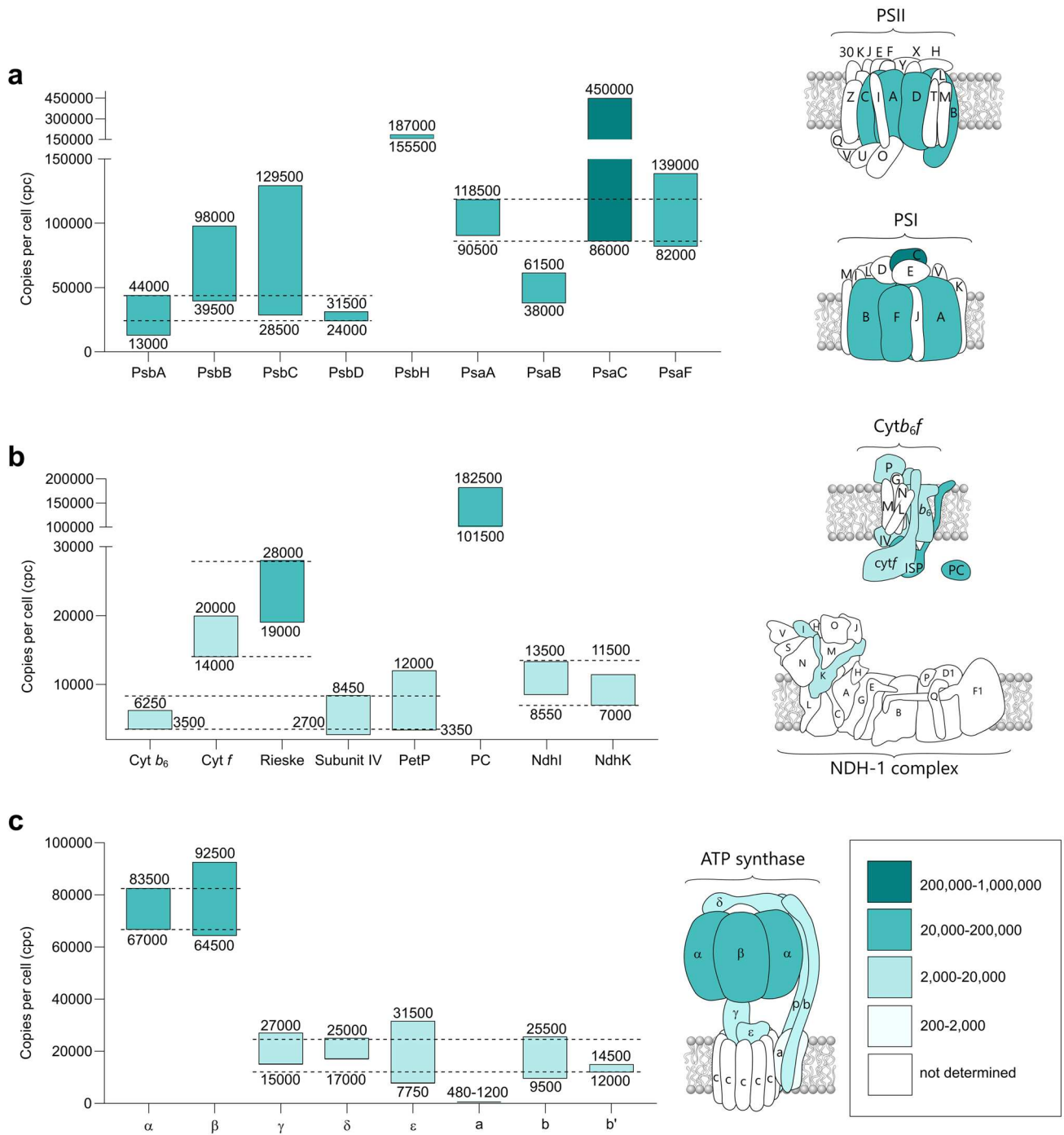
Fig. 1 Cellular levels of protein complexes involved in the conversion of solar to chemical energy. Consensus cpc ranges for the subunits are condensed from the different quantification methods, as described in Results and Discussion, with individual data-points shown in box-plots in Supplementary Fig. S2. The minimum and maximum cpc values are rounded to the nearest 10 (< 1000), 50 (1000–10,000) or 500 (> 10,000) and displayed as bars, shaded according to cpc range, for photosystem II (PSII, PsbA-H), photosystem I (PSI, PsaA-F) (**a**), cytochrome b_6f (cytb_6f), PetP, phycocyanin (PC), photosynthetic NAD(P)H dehydrogenase-like complex type-1 (NDH-1) (**b**) and ATP synthase (**c**). Abundance levels corresponding to the largest extent of overlap between subunits, shown by the horizontal dashed lines, are taken to represent probable ranges for the complexes, explained in Results and Discussion: PSII (24,000–44,000 cpc), PSI (86,000–118,500 cpc), cytb_6f (3350–8450 or 14,000–28,000 cpc), NDH-1 (7000–13,500 cpc), ATP synthase (α, β: 67,000–83,500 cpc; γ, δ, ε, a, b, b': 12,000–25,000 cpc)

2008) where its function appears unrelated to photosynthetic electron transport (Veit et al. 2016a).

The minor subunits, PetG, PetL, PetM and PetN, encoded in *Synechocystis* by smr0010, ssl3803, smr0003 and sml0004 respectively (Schneider et al. 2007) were not identified in our analyses; these proteins are all smaller than 40 residues, hydrophobic and form a single transmembrane helix (TMH). Therefore, their resistance to trypsin digestion and consequent non-detection in these analyses might be expected. The putative regulator of electron transport, PetP (Ssr2998), previously characterized in *T. elongatus* (Rexroth et al. 2014; Veit et al. 2016b), was quantified at 3350–12,000 cpc (Fig. 1b). The lower end of this range coincides with the 3300 cpc determined for PetP in *T. elongatus* by Rexroth et al. (2014).

Plastocyanin (PC, PetE), the copper-containing electron carrier between cytb_6f and PSI is found to be highly abundant at 101,500–182,000 cpc (Fig. 1b). The alternative electron carrier to PC, cytc_6 (PetJ) which is produced in response to growth conditions with low copper levels (García-Cañas et al. 2021) is detected at a low level (Supplementary Data Sets S1 and S2) but, with representation by a single peptide, was not validated for quantification. The dominance of PC over cytc_6 is predictable under the nutrient-rich culture conditions used here; in the presence of Cu, expression of *petJ* is repressed while *petE* expression is induced by a mechanism involving the protease Slr0241 (García-Cañas et al. 2021), not detected here.

Photosystem I

PSI receives electrons from either PC or cytc_6 (see above) and uses solar energy to drive the reduction of Fd, which functions in a wide range of metabolic pathways including NADPH generation in a reaction catalysed by ferredoxin-NADP$^+$ reductase (FNR, see below). NADPH is subsequently involved in, among other processes, the CBB cycle for CO_2 fixation (Lea-Smith et al. 2016; Figs. 2, 3 and 5).

Four PSI subunits were quantified: PsaA–C and PsaF. Figure 1a shows abundance levels that cover the majority of data-points over the 86,000–118,500 cpc range. As in the case of the PSII D1 and D2 subunits, the data-point overlap for PsaA, PsaC and PsaF approximately fits a one subunit per complex stoichiometry (Çoruh et al. 2021). PsaB, appearing to be underestimated at 38,000–61,500 cpc, exemplifies the potential for inaccuracy with MS-based protein quantification resulting from, for example, idiosyncratic proteolysis and/or peptide ionization properties, as detailed in Supplementary Table S1. Our quantification of PSI aligns, at its lower end, with the 63,000–99,000 and 96,000 cpc determined spectrophotometrically by Fujita and Murakami (1987) and Keren et al. (2004) respectively. The latter authors also quoted their measurement of Chl content

at 1.4×10^7 molecules/cell. On the basis that each PSI complex houses 95 Chl molecules (Malavath et al. 2018), 96,000 cpc would account for 9.1×10^6 Chls, approximately 65% of the total cellular content. Assuming the same proportion, our determination of $1.57 \pm 0.04 \times 10^7$ Chl molecules/cell (Supplementary Table S4) correlates with 107,500 cpc of PSI, which is within the range determined by our MS-based quantification.

Photosynthetic NAD(P)H dehydrogenase-like complex type-1

Under conditions of environmental stress that require an increased ATP:NADPH ratio, for example to meet a higher demand for protein synthesis, the proton gradient across the TM, utilized by the ATP synthase complex, can be elevated by cyclic electron transfer (CET; Kramer et al. 2004). One of the CET mechanisms used by cyanobacteria is mediated by photosynthetic NAD(P)H dehydrogenase-like complex type-1 (NDH-1; reviewed by Laughlin et al. 2020; Fig. 1b). In *Synechocystis*, NDH-1 is composed of 19 subunits, distributed between membrane-intrinsic and peripheral arm regions (Pan et al. 2020). In our analysis two subunits located in the latter region, NdhI and NdhK are quantified at 8550–13,500 and 7000–11,500 cpc, respectively (Fig. 1b), consistent with evidence that all NDH-1 subunits occur at one copy per complex (Pan et al. 2020).

ATP synthase complex

The (cyano) bacterial ATP synthase complex (Fig. 1c) comprises two main functional components, one membrane extrinsic and the other embedded in the membrane bilayer (Guo et al. 2019). The membrane-extrinsic, catalytic F_1 component contains α- and β-subunits at three copies each with single-copy γ-, δ- and ε-subunits. The membrane-intrinsic, proton translocating F_O complex contains a single a-subunit and, in *Synechocystis*, 14 c-subunits (Pogoryelov et al. 2007). Forming the peripheral stalk connecting the two sectors are the single-copy b- and b'-subunits.

Here, we determined the ranges 67,000–83,500 cpc for α, β and 12,000–25,500 cpc for γ, δ, ε, b, b', giving a $(\alpha\beta):(\gamma\delta\varepsilon bb')$ ratio of 2.6–7.0 (Fig. 1c). The lower end of this range reflects the known stoichiometry of the ATP synthase complex, as detailed above (Guo et al. 2019). A higher $(\alpha\beta)$ stoichiometry, approaching 7.0, may be accommodated by our quantification of fully assembled, functional complexes together with nascent complexes composed of partially assembled modules. Indeed several F_1 sub-assemblies have been detected in *E. coli*: $\gamma\varepsilon$ (Rodgers and Wilce 2000), $\alpha_3\beta_3\gamma$ (Koebmann et al. 2002) and $\alpha_3\beta_3\gamma\varepsilon$ (Deckers-Hebestreit 2013).

In *E. coli*, ATP synthase subunits were quantified at 2700–3700 cpc for α/β and 600–1700 cpc for γ/δ/ε (Wiśniewski and Rakus 2014), giving a (αβ):(γδε) ratio of 1.6–6.2, in close agreement with the present study. Based on γ/δ/ε cpc, the cellular abundance of ATP synthase complexes in *Synechocystis* is therefore approximately 15–40-fold higher than in *E. coli*. This marked difference in ATP synthase levels between these two organisms may be predictable given their vastly divergent metabolic characteristics.

Biosynthesis

Carboxysomes

Carboxysomes are 100–200 nm icosahedral structures located in the cytoplasm of cyanobacteria (Faulkner et al. 2017), each comprising a self-assembling multi-protein shell that houses two of the Calvin–Benson–Bassham (CBB) cycle enzymes: carbonic anhydrase (CcaA) and ribulose-1,5-bisphosphate carboxylase/oxygenase (RuBisCO). Two types of carboxysomes (α and β) have been defined based on their associated RuBisCO isoforms, with the β-type occurring in *Synechocystis* (Badger et al. 2002). The shell contains pores that selectively allow HCO_3^-, the substrate for CcaA to enter while preventing the exit of CO_2 and the entry of O_2 (Cai et al. 2009). Thus, carboxysomes are nanocompartments in which CO_2 becomes concentrated and O_2, the competitive inhibitor of RuBisCO with respect to CO_2 is excluded.

Six of the seven proteins that comprise the carboxysomal shell are quantified in this study, together with one of the two proteins reported to function in assembly and organization (Cameron et al. 2013). The CcmK1–4 proteins first assemble as homohexamers alongside mixed stoichiometry K1–K2 and K3–K4 heterohexamers, each with a central pore. The hexamers then associate as a single-layer forming the shell facets (Faulkner et al. 2017). In terms of quantification, CcmK1–4 fall into two abundance groups with K1 and K2 at 79,000–169,000 and 61,000–94,500 cpc respectively and, at 10–20-fold lower abundance, K3 and K4 at 2900–8100 and 9400–19,500 cpc (Fig. 2a). These groupings align with earlier observations of K1/2 as major and K3/4 as minor shell proteins (Yeates et al. 2011). CcmL proteins, quantified here at 3550–8850 cpc, are homopentameric and form the carboxysomal vertices (Tanaka et al. 2008). Using the dimensions presented by Faulkner et al. (2017), based on TEM and cryo-EM imaging and assuming regular icosahedral geometry with 20 facets and 12 vertices, we estimate that our quantification of CcmK1 and CcmL would give 11–23 and 59–148 carboxysomes per cell respectively. The EM-based carboxysome count is six on average (Reinhold et al. 1991) therefore the excess shell protein levels are likely due to a substantial population of incomplete carboxysomes,

as described in models for both biogenesis (Cameron et al. 2013) and degradation (Hill et al. 2020).

Like CcmK1–4, the shell protein CcmP oligomerizes around a central pore. However, CcmP is more complex than the single-layer CcmK1–4 since it integrates into the shell as a stacked dimer of trimers. This arrangement not only encloses an internal compartment but also provides a mechanism for gating the central pore (Cai et al. 2013). Assuming six carboxysomes per cell, alongside our quantification at 930–1900 cpc (Fig. 2a), there would be 25–50 of these CcmP gated pores per carboxysome.

Deletion mutants of the seventh shell protein CcmO have confirmed its absolute requirement for carboxysome assembly and that it associates with CcmK1/2 during the encapsulation phase (Rae et al. 2012; Cameron et al. 2013). The hypothesis that CcmO occurs at the facet edges (Rae et al. 2012) might imply that this protein is at least moderately abundant. Unexpectedly, CcmO was not detected in either this or previous (Faulkner et al. 2017) proteomic analyses.

In addition to the outer shell proteins, carboxysomes contain CcmM and CcmN, which are involved in structural organization. CcmM occurs as two isoforms (Cot et al. 2008): (1) the full-length translation product CcmM73 is located within an inner shell where it functions as a scaffold protein interacting with CcmK1-4, CcmL, CcaA and CcmN (Long et al. 2007; Kinney et al. 2012) and (2) the truncated product of an alternative downstream initiation codon CcmM52 which crosslinks RuBisCO in paracrystalline arrays for assembly into the carboxysome interior (Cameron et al. 2013). Our quantification of CcmM at 21,000–44,500 cpc might be expected, given its dual functionality and multiple interaction partners, including possibly 50,000 RuBisCO hexadecamers (see below). However, without the ability to differentiate CcmM73 and CcmM52 by our methodology, further interpretation is not applicable. CcmN, like CcmO (see above) was not detected either here or by Faulkner et al. (2017).

Calvin-Benson-Bassham cycle

The enzymes belonging to the CBB cycle were selected for quantification in this study by referring to https://www.genome.jp/kegg-bin/show_pathway?syn00710 and are shown in Figs. 2b, c. The first step is the conversion of HCO_3^- to CO_2 by carbonic anhydrase (CcaA), quantified here at 2400–9200 cpc (Fig. 2b). Its catalytic unit is a homodimer and, with a $k_{cat} = 3340$ s^{-1}, CcaA potentially generates $4–15 \times 10^6$ CO_2 molecules $cell^{-1}$ s^{-1} (McGurn et al. 2016). This reaction occurs inside carboxysomes (see above) where the second step, in which RuBP is carboxylated by RuBisCO, generates two molecules of glycerate-3-P. RuBisCO is often cited as the most abundant enzyme on Earth and, accordingly the result of our quantification of its
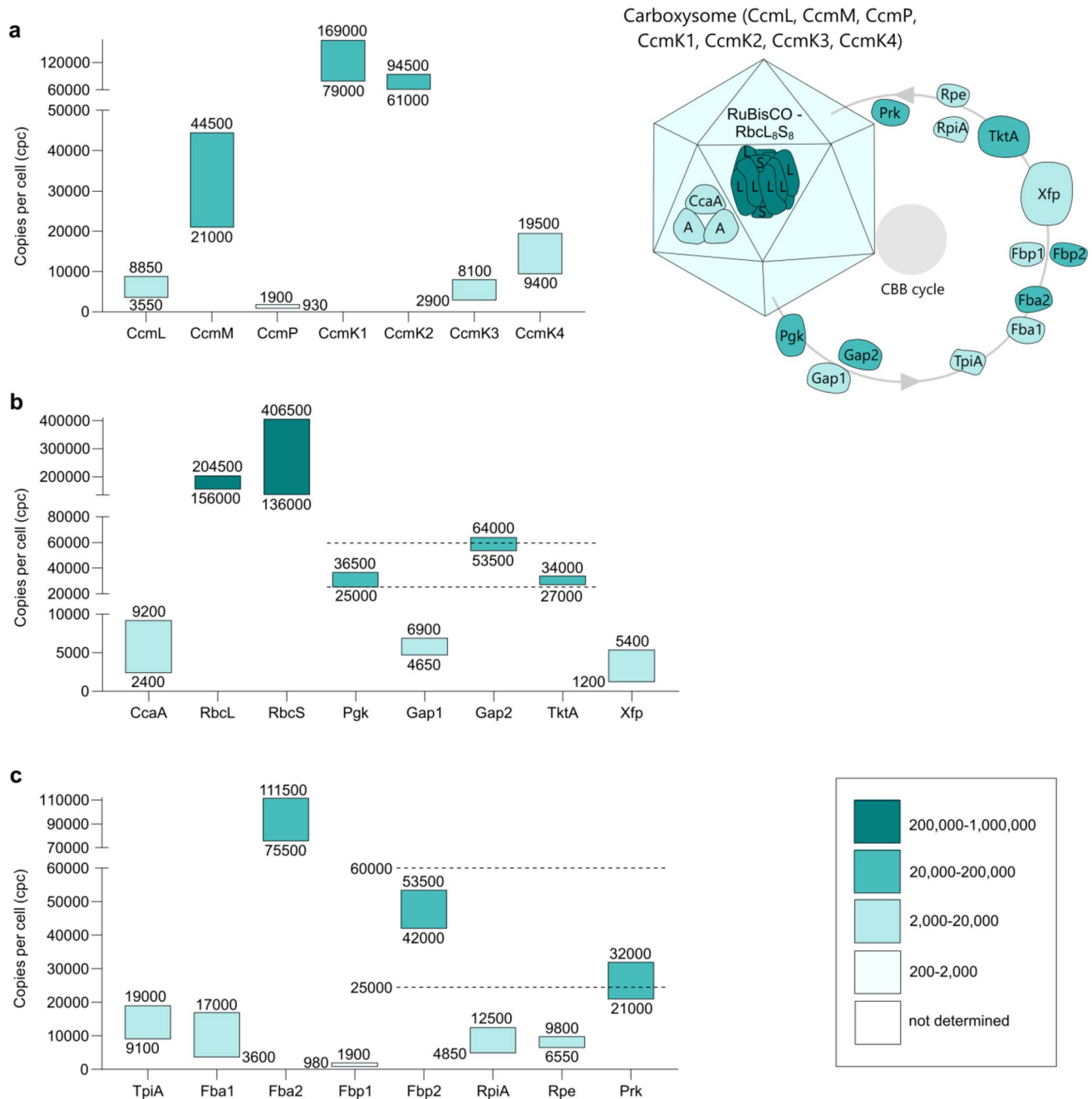
Fig. 2 Cellular levels of carboxysomal proteins and enzymes of the Calvin–Benson–Bassham cycle. Consensus cpc ranges are derived from data-points shown in Supplementary Fig. S3 and displayed as in Fig. 1. Structural carboxysomal proteins (**a**), Calvin–Benson–Bassham cycle enzymes: carbonic anhydrase (CcaA), ribulose-1,5-bisphosphate carboxylase-oxygenase (RuBisCO: large, RbcL and small, RbcS subunits), glycerate-3-phosphate kinase (Pgk), glycer-ate-1,3-phosphate dehydrogenase (Gap1, 2), transketolase (TktA), phosphoketolase (Xfp) (**b**), triose phosphate isomerase (TpiA), fructose-1,6-bisphosphate aldolase (Fba1, 2), fructose-1,6- and sedoheptulose-1,7-bisphosphatase (Fbp1, 2), ribose-5-phosphate isomerase (RpiA), ribulose-3-phosphate epimerase (Rpe), ribulose-5-phosphate kinase (Prk) (**c**). The horizontal dashed lines in (**b**) and (**c**) define a 25,000–60,000 cpc range, explained in Results and Discussion

large (RbcL) and small (RbcS) subunits is 156,000–204,500 and 136,000–406,500 cpc, respectively (Fig. 2b). In the majority of photoautotrophs, including cyanobacteria, RuBisCO is hexadecameric with 8 copies each of the RbcL and RbcS subunits (Andersson et al. 2008). Therefore

the number of active enzyme complexes might approach 50,000 per cell. This very high abundance would mitigate for its slow carboxylation rate, estimated at ~0.7 s⁻¹ per active site in *S. elongatus* (Flamholz et al. 2019). The cpc levels presented here would accommodate the known 1:1

stoichiometry, although the upper extent of the RbcS range at > 400,000 cpc also suggests a two-fold excess over RbcL in vivo. Similarly, a relative LFQ proteomic analysis of *Synechocystis by* Kwon et al. (2013) reported a 1.4-fold excess of RbcS.

Following its formation by RuBisCO, glycerate-3-P exits the carboxysome and the CBB cycle continues in the cytoplasm, ultimately regenerating RuBP. Intermediates downstream of glycerate-3-P in the CBB cycle additionally feed into numerous biosynthetic and metabolic processes (reviewed by Mills et al. 2020). While kinetic parameters for cyanobacterial CBB cycle enzymes are apparently not well represented in the literature (Janasch et al. 2019), some patterns do emerge that align with the quantification results shown in Figs. 2a, b. The ATP- and NADPH-utilizing steps, catalysed by glycerate-3-P kinase (Pgk), glycerate-1,3-phosphate dehydrogenase (Gap2) and ribulose-5-phosphate (Ru5P) kinase (Prk) all occupy an intermediate abundance range of 25,000–60,000 cpc, indicated by horizontal dashed lines in Figs. 2b, c. The alternative dehydrogenase isoform Gap1 principally catalyses the reverse reaction (Koksharova et al. 1998). Its lower abundance, at 4650–6900 cpc may be expected given that Gap1 activity would be counterproductive to flux through the CBB cycle. Metabolomics-based kinetic modelling in *Synechocystis* has revealed that the steps catalysed by Pgk, Prk and another enzyme within the 25,000–60,000 cpc range, fructose-1,6/sedoheptulose-1,7-bisphosphatase (FBP/SBPase, Fbp2) are strong effector reactions in the control of flux through the CBB cycle (Janasch et al. 2019). This role of Fbp2 in flux control was corroborated in *Synechocystis* by Hing et al. (2019) who also identified transketolase (TktA), another enzyme in the same intermediate abundance range, as a key player. Therefore, Pgk, Prk, Fbp2 and TktA may all be targets of the same expression control mechanism in response to ambient growth conditions. In their analysis, Janasch et al. (2019) additionally identified RuBP, FBP and SBP as intermediates that would perturb the overall steady-state stability of the CBB cycle if their cytosolic concentrations were to increase beyond a critical level. Limiting the production of RuBP, FBP and SBP might be mediated by restricting the abundance levels of upstream enzymes. In support of this hypothesis, ribose-5-phosphate isomerase A (RpiA) and ribulose-3-phosphate epimerase (Rpe), which convert ribose-5-phosphate (R5P) and xylulose-5-phosphate (Xu5P) respectively into Ru5P, the RuBP precursor, are both quantified in a relatively low abundance range (4850–12,500 and 6550–9800 cpc respectively; Fig. 2c). Similarly, production of SBP precursors glycerone-phosphate (also named dihydroxyacetone phosphate) and erythrose-4-phosphate (E4P) may be limited by the relatively low abundance of triose phosphate isomerase (TpiA) and phosphoketolase (Xfp) at 9100–19,000 and 1200–5400 cpc, respectively.

Like Gap1/2, other CBB enzymes occur as two isozymes. The reaction catalysed by RpiA, described above, is also potentially mediated by RpiB (see KEGG link above). This apparently uncharacterized protein is not detected in this analysis, prompting the conclusion that RpiA is probably the only R5P isomerase isozyme produced by *Synechocystis* under the growth conditions used here. In the case of fructose-1,6-bisphosphate (FBP) aldolase which converts G3P + glycerone-P to FBP and E4P + glycerone-P to SBP, both Fba1 and Fba2 isozymes are quantified at widely differing ranges: 3600–17,000 and 75,500–111,500 cpc, respectively (Fig. 2c), again highlighting the dominance of one isozyme over the other. This abundance pattern is repeated with quantification of Fbp1 and Fbp2 at 980–1900 and 42,000–53,500 cpc respectively. While these isozyme abundance level differences cannot be rationalized without experiments to examine the effects of different growth conditions, there is evidence that deployment of alternative CBB cycle isozymes in *Synechocystis* provides a mechanism for acclimation to environmental CO_2 levels that extends beyond transcriptional control (Jablonsky et al. 2016).

Ferredoxin-dependent processes

There are nine ferredoxins (Fds) in *Synechocystis*: Ssl0020 is the isoform that mediates electron transfer from the Fe-S centers on the PsaC subunit of PSI (Yu et al. 1995). Like PC, Fd is highly abundant: although its quantification is below the validation threshold with two quantotypic tryptic peptides, it may occur above 200,000 cpc (Fig. 3a), exceeding the abundance of PSI by factor of 2–3 (cf. Figure 1a). The 10^5 order of magnitude for the copy number of Fd in *Synechocystis* cells has been corroborated by quantitiative immunoblotting (Moal and Lagoutte 2012). This high cellular level reflects the numerous Fd-dependent metabolic processes that exist in cyanobacteria. Of particular relevance to photosynthesis, the ferredoxin NADP$^+$ reductase (FNR), which catalyses the production of NADPH for CO_2 fixation (Cassier-Chauvat and Chauvat 2014), occurs in both full-length, and truncated (FNR$_s$, with alternative initiation at M113) isoforms (Thomas et al. 2006). We quantified FNR with peptides identified from both N- and C-sides of M113 (Supplementary Data Sets S5 and S6). Although the two isoforms would, therefore, be indistinguishable in this analysis, we assume that FNR$_s$ would be absent under the photoautotrophic growth conditions used here since it is only detected during heterotrophic metabolism (Thomas et al. 2006). With FNR at 20,500–30,500 cpc (Fig. 3a), the PSI:FNR ratio would be approximately 4:1, which again aligns closely with a quantitative immunoblot assay by Moal and Lagoutte (2012).

In addition to these photosynthesis-related processes, Fd is required for at least nine other metabolic processes
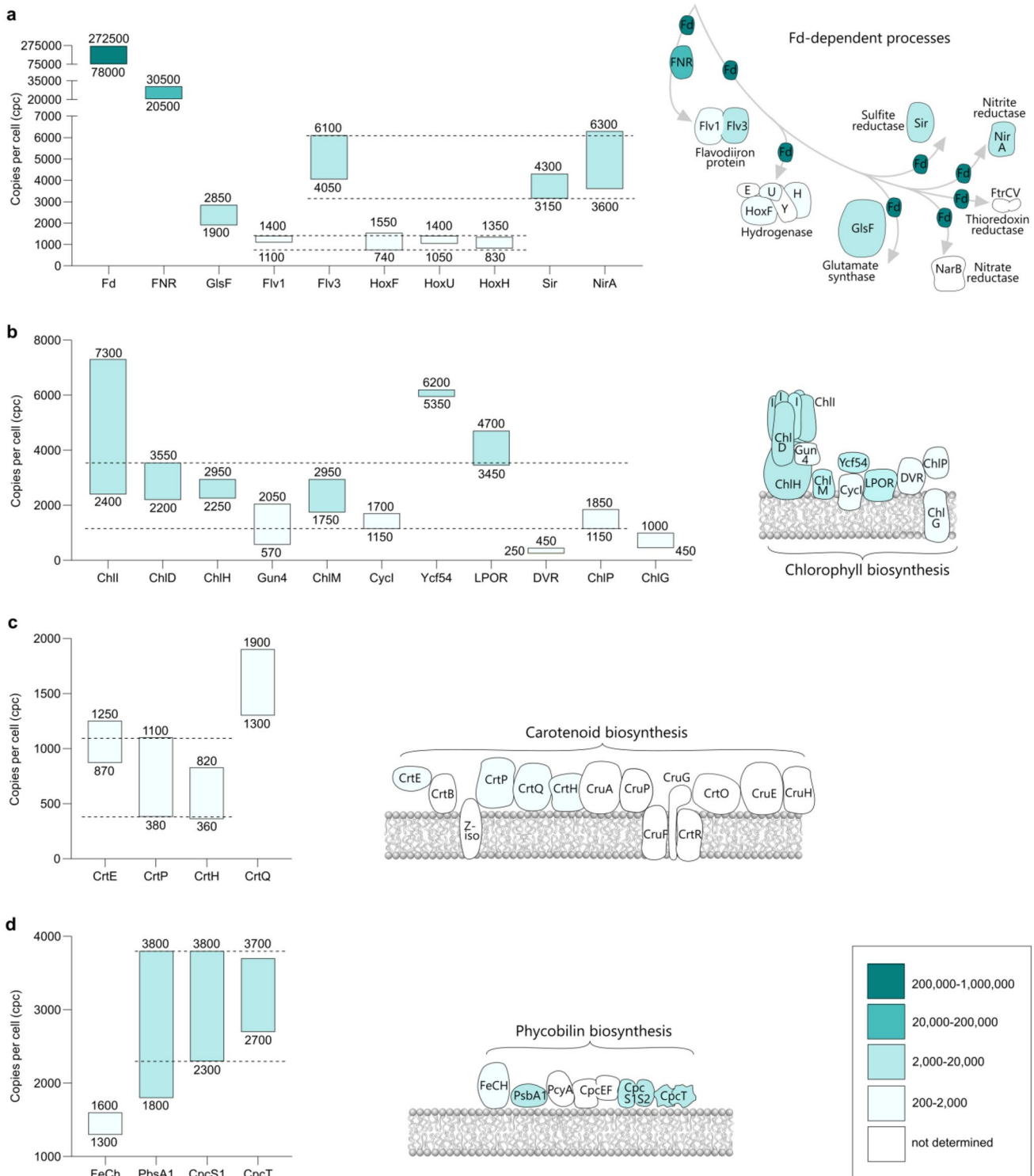
in cyanobacteria (Lea-Smith et al. 2016). Figure 3a shows quantification results for eight of these including glutamate synthase 2 (GlsF, encoded by *gltS*) at 1900–2850 cpc. The remaining seven fall into two abundance groups shown by dashed lines in Fig. 3a. Three of the five subunits of the bidirectional hydrogenase, HoxF, HoxU and HoxH are

quantified here at 740–1550, 1050–1400 and 830–1350 cpc (Fig. 3a, lower abundance group), consistent with the known subunit stoichiometry (Vignais and Billoud 2007). The flavodiiron protein (FDP), comprising Flv1 and Flv3 subunits, functions as a heterodimer (Allahverdiyeva et al. 2011). In this case, our analysis is at odds with a

◄**Fig. 3** Cellular levels of enzymes and auxiliary proteins involved in biosynthesis. Consensus cpc ranges are derived from data-points shown in Supplementary Fig. S4 and displayed as in Fig. 1. Ferredoxin (Fd) and Fd-dependent enzymes: ferredoxin-NADP$^+$ reductase (FNR), glutamate synthase 2 (GlsF), flavodiiron protein (Flv1/3), bidirectional hydrogenase (HoxF, U, H), sulphite reductase (Sir), nitrite reductase (NirA) (**a**), enzymes and auxiliary proteins in the Mg-branch of the chlorophyll *a* biosynthesis pathway: Mg-chelatase (ChlI, ChlD, ChlH, Gun4), Mg-protoporphyrin IX methyltransferase (ChlM), O_2-dependent Mg-protoporphyrin IX methyl ester cyclase (CycI, Ycf54), light-dependent protochlorophyllide oxidoreductase (LPOR), 8-vinyl reductase (DVR), geranylgeranyl reductase (ChlP), chlorophyll *a* synthase (ChlG) (**b**), enzymes in the carotenoid biosynthesis pathway: geranylgeranyl pyrophosphate synthase (CrtE), phytoene desaturase (CrtP), prolycopene isomerase/CRTISO (CrtH), ζ-carotene desaturase (CrtQ) (**c**), enzymes in the phycobilin biosynthesis pathway: ferrochelatase (FeCh), heme oxygenase 1 (PbsA1), chromophore lyase (CpcS1, CpcT) (**d**). The horizontal dashed lines, explained in Results and Discussion, define in: (**a**) 740–1400 and 3150–6100 cpc, (**b**) 1150–3550 cpc, (**c**) 380–1100 cpc and (**d**) 2300–3800 cpc

1:1 stoichiometry by revealing levels of 1100–1400 cpc, in the lower abundance group for Flv1 and 4050–6100 cpc in the higher abundance group for Flv3. The observation that Flv3 is substantially more abundant than Flv1 does however align with more recent evidence of FDP activity by Flv3 oligomers in addition to Flv1/3 heterodimers (Mustila et al. 2016). Other Fd-dependent enzymes in the higher abundance group are sulfite reductase (Sir) at 3150–4300 cpc and nitrite reductase (NirA) at 3600–6300 cpc (Fig. 3a),. The enzyme that acts upstream of NirA, nitrate reductase (NarB), is not detected in this analysis despite being essential for growth in a culture medium containing nitrate as the sole nitrogen source (Baebprasert et al. 2011), as used in this study. Two subunits of the nitrate transporter complex NrtA (Sll1450) and NrtC (Sll1452) are identified (Supplementary Data Sets S1 and S2), implying the cells' probable competency in importing nitrate from the medium. In addition, not quantified here is ferredoxin–thioredoxin reductase; the catalytic subunit FtrC is identified with two tryptic peptides, below the validation threshold for LFQ, but the second subunit, FtrV, is not detected.

The biosynthetic pathway for chlorophyll *a*

Magnesium-chelatase The biosynthesis of Chl *a* is carried out by a series of enzymes and auxiliary proteins (Fig. 3b), starting with the magnesium-chelatase (MgCh) enzyme complex. MgCh catalyses the ATP-dependent insertion of Mg^{2+} into protoporphyrin IX, which is also the substrate for ferrochelatase (FeCh) that produces heme. Thus, the insertion of Mg^{2+} or Fe^{2+} represents a branchpoint in tetrapyrrole biosynthesis (reviewed by Bryant et al. 2020).

MgCh is associated with the cytoplasmic/stromal surface of TMs (Kopečná et al. 2015; Farmer et al. 2019), as depicted in Fig. 3b, and comprises three core subunits: (i) the AAA$^+$ ATPase ChlI (Fodje et al. 2001) which provides the free energy for Mg^{2+} chelation (Reid and Hunter 2004), (ii) ChlD, an allosteric regulator (Adams and Reid 2013) that also transmits the energy released by ATP hydrolysis by ChlI (Adams et al. 2016; Farmer et al. 2019) to (iii) ChlH where the active site resides (Karger et al. 2001; Sirijovski et al. 2008; Adams et al. 2020). Quantification reveals that data-points for ChlI cover a 2400–7300 cpc range while ChlD and ChlH levels are confined to 2200–3550 and 2250–2950 cpc, respectively (Fig. 3b). On the assumption that the abundance range shown by ChlD/H represents a 1:1 molar ratio for these subunits in the active MgCh complex (Farmer et al. 2019), then the level of ChlI in relation to ChlD/H is either the same or only higher by a factor of 2–3. Given that the active MgCh probably comprises multiple copies of ChlI, based on structural evidence that ChlI associates into hexamers (Gao et al. 2020) or heptamers (Reid et al. 2003), it appears that the number of fully-assembled, active MgCh complexes may be limited by the availability of ChlI subunits to 500–1200 per cell, sufficient to produce 7–16 molecules of Mg-protoporphyrin IX (MgP$_{IX}$) s^{-1} cell^{-1}, based on a k_{cat} of 0.013 s^{-1} (Reid and Hunter 2004; Viney et al. 2007). Association of the auxiliary MgCh subunit Gun4 is not an absolute requirement for activity in vitro but does enhance the rate of MgP$_{IX}$ formation by a factor of 3–10 (Larkin et al. 2003; Davison et al. 2005; Davison and Hunter 2011; Adams et al. 2016). We quantified Gun4 at 570–2050 cpc (Fig. 3b), which aligns with the 500–1200 cpc range suggested for the number of active MgCh complexes per cell. If MgCh binds Gun4 in a 1:1 ratio, the rate of MgP$_{IX}$ generation may therefore approach 160 s^{-1} cell^{-1}.

Mg-protoporphyrin IX methyltransferase Following the insertion of Mg^{2+}, MgP$_{IX}$ is converted to Mg-protoporphyrin IX monomethyl ester (MgPME) by Mg-protoporphyrin IX methyltransferase (ChlM). The production of MgPME occurs with $k_{cat} = 57$ s^{-1} (Shepherd and Hunter 2004) which, alongside our quantification of ChlM at 1750–2950 cpc (Fig. 3b), equates to 99,750–168,150 s^{-1} cell^{-1} thereby exceeding the rate of MgP$_{IX}$ production by a factor of > 1000. This marked difference may represent a mechanism for preventing the accumulation of MgP$_{IX}$ and therefore its potentially cytotoxic effects (Tanaka and Tanaka 2007).

O_2-dependent Mg-protoporphyrin IX methyl ester cyclase In the third step of Chl biosynthesis, the C13 methyl-propionyl sidechain of MgPME is cyclized by O_2-dependent Mg-protoporphyrin IX methyl ester cyclase to form the fifth

isocyclic (E) ring of 3,8-divinyl protochlorophyllide *a* (DV-PChlide). The presence of the E ring induces a change in the absorption profile, which transforms the red color of the substrate to a green product (Chen et al. 2021). The cyclase has two isoforms in *Synechocystis*, CycI and CycII, which share 56.7% sequence identity and are encoded by sll1214 and sll1874, respectively. Consistent with the normal culture aeration used here, we identified CycI at 1150–1700 cpc (Fig. 3b) as the only cyclase isoform present. CycII, which is synthesized in addition to the constitutive CycI under low O_2 (Minamizak et al. 2008; Peter et al. 2009), was below the limit of detection in all analyses. The k_{cat} of 0.015 s^{-1} measured by Chen et al. (2021) for CycI is comparable to that of MgCh at 0.013 s^{-1} (determined in the absence of Gun4), giving a potential rate of MgPME to DV-PChlide conversion of 17–26 s^{-1} $cell^{-1}$.

Like MgCh with Gun4, CycI also associates with an auxiliary protein, Ycf54, in *Synechocystis* (Hollingshead et al. 2012) and plants (Bollivar et al. 2014; Herbst et al 2018). Although the structural elements in Ycf54 that mediate its association with CycI have been characterized (Hollingshead et al. 2017), its precise role in MgPME cyclase activity is not yet defined. While our analysis shows that the Gun4 copy number appears to be in an approximate 1:1 ratio with that of assembled MgCh complexes (see above), Ycf54, at 5350–6200 cpc (Fig. 4b) is 3–fivefold more abundant than CycI. This higher stoichiometry may reflect evidence that, although CycI is membrane-associated (Tottey et al. 2003; Rzeznicka et al. 2005; Allen et al. 2008; Hollingshead et al. 2012), Ycf54 is located in both soluble and membrane fractions (Hollingshead et al. 2012).

Protochlorophyllide oxidoreductase (POR) Following DV-PChlide formation, the next two steps in the Chl biosynthesis pathway result in the reduction of the C17=C18 and C8-vinyl double bonds. In cyanobacteria, POR exists as two structurally unrelated versions: light-dependent (LPOR) and light-independent or dark-operative (DPOR) (Reinbothe et al. 2010). The latter is composed of three subunits: ChlN, ChlB, and ChlL, and none of these was detectable in our analyses (Supplementary Data Sets S1 and S2). This finding is expected for the growth conditions used here since DPOR activity is inhibited by O_2 at > 3% and the expression of its subunits is induced only under anaerobic conditions (Yamazaki et al. 2006). LPOR is a single subunit enzyme that uses the energy from a photon absorbed by its substrate, DV-PChlide, to acquire H (with two electrons) from NADPH and a proton from a conserved Tyr residue (Heyes et al. 2006). The analysis presented in Fig. 3b reveals an abundance range of 3450–4700 cpc. A $k_{cat} = 0.027$ s^{-1} (Zhang et al. 2021) gives potential production rates for DV-Chlide of 93–127 s^{-1} $cell^{-1}$, thereby exceeding the upstream cyclase step by a factor of 4–7. As suggested for the MgP_{IX}

to MgPME conversion, the LPOR substrate DV-PChlide is potentially hydrogenated in the light to form DV-Chlide faster than it can accumulate.

8-Vinyl reductase In the next reduction step, catalysed by DV-(P)Chlide 8-vinyl reductase (DVR), the C8 vinyl group of DV-Chlide is converted to ethyl, producing (monovinyl) chlorophyllide (Chlide). DVR, encoded by slr1923 in *Synechocystis* (Islam et al. 2008; Ito et al. 2008), is detectable in both membrane and soluble fractions (Canniffe et al. 2014). Despite its wide distribution, DVR was quantified at the lowest abundance of all the Chl biosynthesis-associated proteins at < 500 cpc (Fig. 3b). To our knowledge, there are as yet no published steady state activity measurements for cyanobacterial DVR, therefore, the potential cellular rate of DV-Chlide to Chlide conversion cannot currently be estimated.

Geranylgeranyl reductase and chlorophyll *a* synthase The final two steps in Chl biosynthesis can occur in either order (Soll et al. 1983; Proctor et al. 2022a). Geranylgeranyl reductase (ChlP) catalyses the hydrogenation of three C=C double bonds on the C_{20} isoprenoid geranylgeranyl pyrophosphate (GGPP) to produce phytyl pyrophosphate. The phytyl group is then attached via an ester linkage to the C17 propionate sidechain on Chlide by Chl *a* synthase (ChlG). Alternatively, ChlG can first attach a geranylgeranyl group to Chlide for subsequent reduction to phytyl by ChlP. ChlP is probably active on the cytosplasmic surface of the TM, whereas ChlG is predicted to be membrane-intrinsic (Gaubier et al. 1995) with up to nine TMHs (Proctor et al. 2022a). ChlP was quantified at 1150–1850 cpc, the sixth Chl biosynthesis pathway component to fall into the shared 1150–3550 cpc range indicated by horizontal dashed lines in Fig. 3b. ChlG was revealed as a member of the lower abundance group of Chl synthesis pathway components, falling in between CycI and DVR, at 450–1000 cpc (Fig. 3b). Since, to our knowledge, there are currently no published k_{cat} measurements for either ChlP or ChlG, their potential cellular catalysis rates remain undetermined.

The carotenoid biosynthesis pathway

Carotenoids are membrane-intrinsic isoprenoids synthesized by all oxygenic photoautotrophic organisms, where they play roles in the function, assembly and stability of complexes including PSII (Umena et al. 2011), PSI (Jordan et al. 2001), cytb_6f (Malone et al. 2019) and NDH-1 (Schuller et al. 2019). Recently, structures of some of these complexes from *Synechocystis* have been determined, revealing the positions of the carotenoids (Malavath et al. 2018; Gisriel et al. 2022; Proctor et al. 2022b). Carotenoids are also essential for photoprotection, quenching ROS-generating Chl triplet states

and superoxide (Cogdell et al. 2000), and in cyanobacteria the photoactive orange carotenoid protein (OCP) is involved in thermal dissipation of excess energy from the phycobilisome antenna (Muzzopappa and Kirilovsky 2020).

Carotenoid biosynthesis (summarized in Fig. 3c and reviewed by Canniffe and Hitchcock (2021)) commences with the condensation of the products of the 2-C-methyl-D-erythritol 4-phosphate (MEP) pathway isopentenyl pyrophosphate (IPP) and dimethylallyl pyrophosphate (DMAP) producing geranyl pyrophosphate (GPP). In oxygenic phototrophs this reaction, together with two subsequent additions of IPP to GPP to produce GGPP, are catalysed by the GGPP synthase (CrtE). Subsequently, two molecules of GGPP are condensed to generate 15-*cis*-phytoene by phytoene synthase (CrtB), which then undergoes a series of desaturations and isomerizations resulting in the production of all-*trans*-lycopene, the common precursor of the major carotenoid species utilized by *Synechocystis*, namely β-carotene, myxoxanthophyll, echinenone, zeaxanthin and synechoxanthin (Lagarde and Vermaas 1999; Graham et al. 2008).

In our analysis, CrtE, which is also required for Chl biosynthesis, is quantified, along with phytoene desaturase (CrtP), ζ-carotene desaturase (CrtQ) and the prolycopene isomerase CRT-ISO (CrtH), all of which occur early in the pathway in the synthesis of all-*trans*-lycopene. Figure 3c shows that CrtE, CrtP and CrtH occur at abundance levels in the 380–1100 cpc range (horizontal dashed lines), while CrtQ is higher at 1300–1900 cpc. In addition to CrtE, CrtP, CrtQ and CrtH, the other enzymes required to generate all-*trans*-lycopene are CrtB and ζ-carotene isomerase (Z-ISO). A *Synechocystis crtB* mutant cannot synthesize carotenoids, is light sensitive and lacks functional PSII (Sozer et al. 2010), suggesting the enzyme is likely to be present just below the detection limit. Given that the cells used here were grown under constant illumination, the known photolability of the 15-*cis* bond of 9,15,9′-tri-*cis*-ζ-carotene (Li et al. 2007) may explain non-detection of the *Synechocystis* Z-ISO (Slr1599; Proctor et al. 2022c), although in plants Z-ISO is important in both "dark" and light-exposed tissues (Chen et al. 2010). Our detection of CrtH, the other carotenoid isomerase, suggests photoisomerization alone is insufficient in the case of the second carotenoid isomerization step; a *Synechocystis crtH* mutant produces normal carotenoids under light conditions due to photoisomerization of the *cis*-bonds in prolycopene, albeit at different ratios to the wild-type organism (Masamoto et al. 2001).

The remaining eight enzymes are either not synthesized under the culture conditions used here or occur at < 200–500 cpc. The major lycopene cyclase CruA (Xiong et al. 2017) is identified but at levels below the threshold for quantification (Supplementary Data Sets S1 and S2), whereas CruP, the lycopene cyclase function of which is controversial (Maresca et al. 2007; Liang et al. 2008), is not detected. Similarly,

CruF and CruG, specific to myxoxanthophyll biosynthesis (Graham and Bryant 2009), CruE and CruH, required for synthesis of synechoxanthin (Graham and Bryant 2008), and CrtO, the ketolase for echinenone and 3-hydroxy-echinenone biosynthesis (Fernández-González et al. 1997) are not detected, nor is CrtR, which adds the hydroxyl groups to the β-rings of zeaxanthin, myxoxanthophyll and 3-hydroxy-echinenone (Lagarde and Vermaas 1999).

Levels below the threshold of identification for carotenoid biosynthesis enzymes were also apparent in two previous proteomic studies that employed sub-cellular fractionation to potentially enhance proteomic coverage (Xu et al. 2021; Baers et al. 2019). This low copy number may be a consequence of the low turnover of carotenoids under moderate illumination conditions and/or extremely efficient enzymes meaning high cellular levels are not required.

The phycobilin biosynthesis pathway

Bilins, linear tetrapyrroles derived from heme, are light-harvesting chromophores covalently attached to phycobiliproteins, which assemble to form the phycobilisome antenna complex (Dominguez-Martin et al. 2022). The biosynthesis pathway of bilins, reviewed by Bryant et al. (2020), is common with that of Chls up to protoporphyrin IX, where it diverges from the branch initiated by the insertion of Fe^{2+} catalysed by ferrochelatase (FeCh, HemH) to produce heme. Heme oxygenase (Hox) then cleaves the heme macrocycle to produce the linear molecule biliverdin IXα, which is subsequently converted to a bilin via a Fd-dependent bilin reductase; *Synechocystis* produces only phycocyanobilin (PCB). We quantify FeCh (Slr0839; 1300–1600 cpc) and HoxI (PbsA1, 1800–3800 cpc), while the PCB-ferredoxin oxidoreductase (PcyA) is detected but present at < 500 cpc. As expected, Hox2 (PbsA2), which is produced under microoxic conditions (Yilmaz et al. 2010), is not identified.

The attachment of phycobilins to specific cysteine residues of phycobiliproteins requires specific bilin lyases (Scheer and Zhao 2008). In cyanobacteria such as *Synechocystis* and *Synechococcus* sp. PCC 7002, three PCBs are attached to a phycocyanin heterodimer, one to CpcA by a heterodimeric lysase comprised of CpcE and CpcF (Fairchild et al. 1992), one to CpcB by a CpcS/CpcU family lyase (Saunée et al. 2008) and one to CpcB by a CpcT family lyase (Shen et al. 2006). CpcS/CpcU also attach PCB to the core allophycocyanin antenna subunits ApcA, ApcB, ApcD and ApcF (Zhao et al. 2007). We quantify CpsS1 (CpcU, 2300–3800 cpc) and CpcT (2700–3700 cpc) but not CpcE, CpeF or CpcS2 (CpcS), suggesting these are present at < 500 cpc.

An alternative fate of biliverdin Ixα is reduction to bilirubin by the pyridine nucleotide-dependent biliverdin reductase (BvdR); the *Synechocystis* enzyme is quantifed

by only 1–2 peptides at < 500 cpc (Supplementary Data Set S4). Although not a direct component of the phycobiliosme, bilirubin is suggested to act as a ROS scavenger (Hayes and Mantle 2009) and BvdR is important for normal phycobiliprotein biosynthesis in *Synechocystis* (Schluchter and Glazer 1997).

Photosystem assembly and repair

Coordination of chlorophyll and photosystem II biosynthesis

ChlG and HliD As stated above, the step in the Chl biosynthesis pathway in which either a geranylgeranyl or phytyl chain is ester-linked to the Chlide macrocycle is catalysed by ChlG. Immunoprecipitation (IP) experiments employing FLAG-tagged ChlG have shown that this membrane-intrinsic enzyme co-isolates with the single-TMH proteins HliC (Niedzwiedzki et al. 2016) and HliD (Chidgey et al. 2014), two of the four high light-inducible proteins (Hlips) present in *Synechocystis* (HliA-D; Komenda and Sobotka 2012). The ChlG-HliC/D complex also incorporates Chl and carotenoids (Chidgey et al. 2014; Niedzwiedzki et al. 2016), implicating HliC and HliD in photoprotection specifically during PSII, but not PSI (see below), assembly in which the delivery of Chl is coordinated with the co-translational insertion of nascent apoproteins into the membrane (Chidgey et al. 2014; Knoppová et al. 2014). According to our analyses, the abundance of ChlG is 450–1000 cpc (Fig. 3b) with HliD 3–sevenfold higher at 2000–3200 cpc (Fig. 4a). HliC was also identified in this study (Supplementary Data Sets S1 and S2) however, recovery of its single proteotypic tryptic peptide from artificial SIL standard proteins proved non-reproducible during initial tests (results not shown) and LFQ would be below the validation threshold with < 3 peptides. The greater abundance of HliD over ChlG is supported by the observation that carotenoids only bind to HliC/D dimers, not monomers (Shukla et al. 2018), implying that the functional units of these Hlips are dimers. The detection of ChlG- and HliD-containing complexes at > 100 kDa by native-PAGE/immunoblot analysis (Proctor et al. 2020) further suggests that PSII assembly centers may comprise multiple copies of ChlG and HliC/D dimers.

Ycf39 An additional protein co-isolating with Flag-ChlG in IP analysis is Ycf39 (Slr0399; Chidgey et al. 2014), although its interaction with the complex is lost under high-light conditions (Proctor et al. 2018). Ycf39 is predicted to be hydrophilic and its interaction with the membrane-intrinsic ChlG-HliC/D complex is on the TM cytoplasmic surface (Knoppová et al., 2014). IP analysis using FLAG-tagged Ycf39 showed that its direct binding partner is dimeric HliC/D (Staleva et al., 2015) and native-PAGE/immunoblot analysis confirmed the association of Ycf39 with early intermediates in the PSII assembly pathway (Knoppová et al., 2014, 2022; Heinz et al. 2016; Konert et al. 2022). Ycf39, is quantified here at 1200–1800 cpc (Fig. 4a), therefore HliD alone outnumbers Ycf39 by a factor of two, highlighting the possibility that all copies of Ycf39 are bound to Hlip dimers.

YidC and SecY The identification of ChlG-HliC/D-Ycf39 complexes highlights the PSII assembly process in terms of Chl delivery and photoprotection. The additional detection of the membrane insertase YidC in FLAG-ChlG IP analyses (Chidgey et al. 2014; Niedzwiedzki et al. 2016) establishes the direct link with co-translational integration of PSII apoproteins into the TM. While the ChlG-HliC/D-Ycf39 complex is evidently specific to PSII assembly (Knoppová et al. 2014, 2022; Pascual-Aznar et al. 2021), YidC participates in the co-translational insertion of a wide range of membrane-intrinsic proteins (Kudva et al. 2013). YidC was quantified here at 1000–3350 cpc (Fig. 4a), coincident with the 2500–3000 cpc determined in *E. coli* (Urbanus et al. 2002; Kudva et al. 2013). SecY, the only subunit of the SecYEG translocon identified here, is quantified at 110–830 cpc. Again, this range is in close agreement with the 200–600 cpc in *E. coli* (Kudva et al. 2013). The perhaps unexpectedly low abundance of these proteins in *Synechocystis* may be rationalized on the basis that a chaperone-type function is similar to catalysis in that, after membrane insertion of the substrate protein, YidC and SecYEG are released and available to bind a new substrate. Furthermore, a recent fluorescent imaging study of mRNA sequences mapping to PsaA and PsbA has revealed that translation sites for these membrane-integral PS subunits are not widely distributed but instead confined to the interior cytosol-facing surface of the TMs (Mahbub et al. 2020). TM-intrinsic protein insertion appears therefore to be localized and the levels of YidC and SecYEG may reflect this.

Thylakoid membrane biogenesis and photosystem II assembly

CurT The characteristic morphology of thylakoids in cyanobacteria is dependent on CurT, an integral membrane protein that induces membrane curvature (Heinz et al. 2016). Accordingly, inactivation of *curT* results in the development of aberrant TM structure and additionally a 50% reduction in PSII accumulation compared to wild-type. This effect on PSII levels is accompanied by the elimination of the biogenesis centers, more recently referred to as 'convergence zones' (Rast et al. 2019), implicating CurT in the formation of these features as part of normal TM morphology (Heinz et al. 2016). Quantification of CurT in this study indicates the possibility of cellular levels approaching 140,000 cpc (Fig. 4a). Imaging by both immunofluorescence and immu-
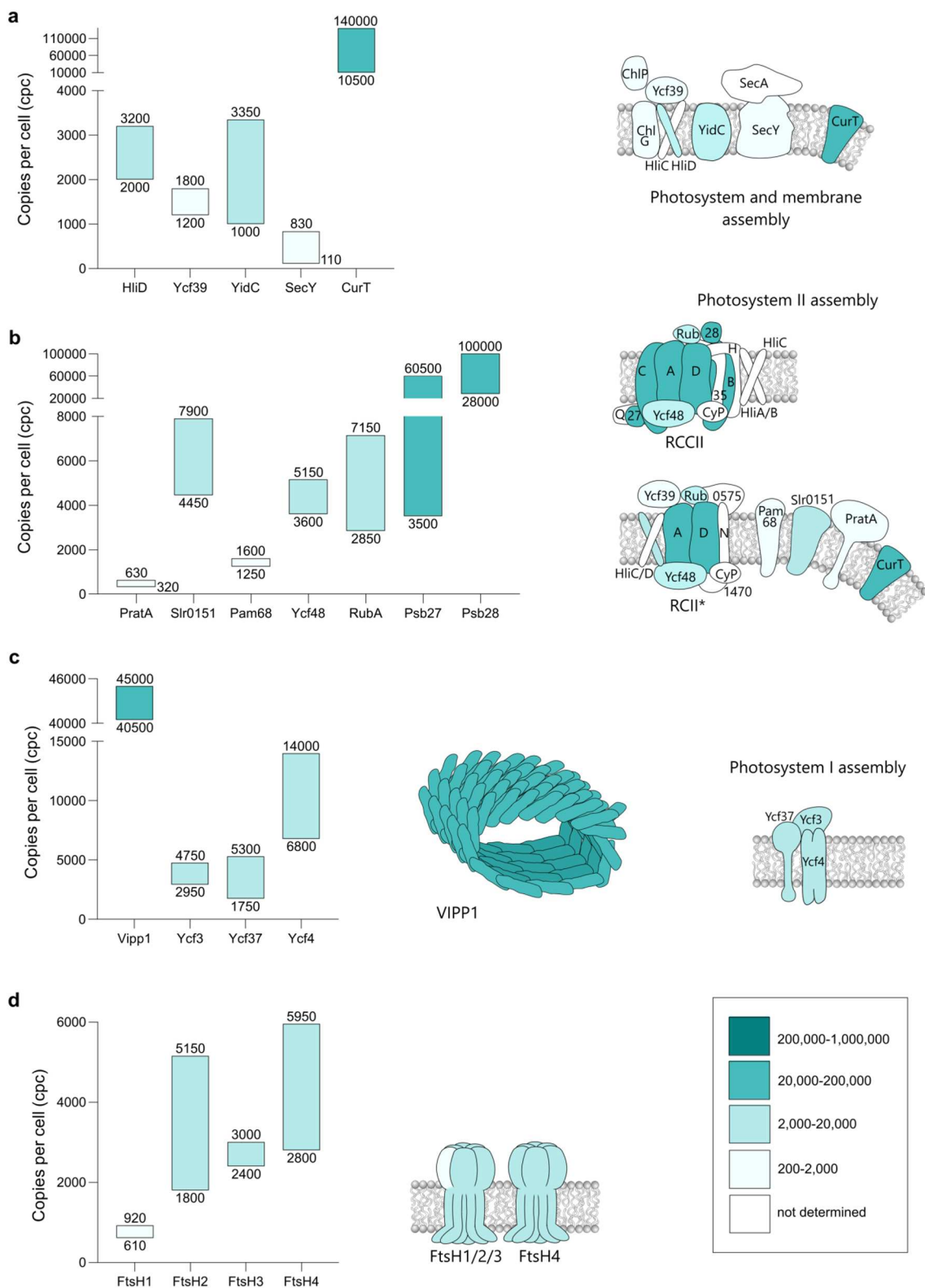
Fig. 4 Cellular levels of assembly factors and enzymes involved in thylakoid membrane biogenesis and photosystem assembly/repair. Consensus cpc ranges are derived from data-points shown in Supplementary Fig. S5 and displayed as in Fig. 1. Proteins involved in the coordination of chlorophyll and PSII biosynthesis (**a**), proteins involved in thylakoid membrane biogenesis and PSII assembly (**b**), proteins involved in thylakoid membrane biogenesis and PSI assembly (**c**), and ATP-dependent zinc metalloproteases: membrane protein quality control and PSII repair (**d**)

nogold labelling supports this finding since CurT is detectable, not only in association with convergence zones but also throughout the TM on both concave and convex surfaces (Heinz et al. 2016).

PratA, Pitt and Slr0151 Specifically localized to the convergence zones where they function as PSII assembly factors are three tetratricopeptide repeat (TPR) proteins: PratA (Slr2048; Klinkert et al. 2004), Pitt (Slr1644; Schottkowski et al. 2009) and Slr0151 (Rast et al. 2016). Using high-resolution cryo-electron tomography, it has been demonstrated that, within the convergence zones, membranes continuous with the TM are in close contact with the CM (Rast et al. 2019). This juxtaposition enables a mechanism whereby PratA delivers Mn^{2+} from the periplasm to the membrane-integrated PsbA precursor (pD1; Stengel et al. 2012). The level of PratA was quantified here at 320-630 cpc (Fig. 4b).

Pitt (encoded by slr1644) is anchored in the TM via an N-terminal TMH and inactivation of slr1644 was shown to reduce the accumulation of LPOR (see above) by 70% (Schottkowski et al. 2009). These authors suggested that the association of LPOR with the TM might be via its binding to Pitt. With representation by only two tryptic peptides, Pitt was not validated for quantification. However, iBAQ abundance scores are consistent with a level of Pitt at < 500 cpc (Supplementary Data Set S4). Our quantification of LPOR at 3450–4700 cpc (see above), up to tenfold more abundant than Pitt, would align with the further idea of an LPOR-Pitt membrane-attachment complex that directs a relatively small LPOR sub-population to the convergence zone for an, as yet unknown function.

Slr0151 has been characterized as functioning in PSII biogenesis (Rast et al. 2016) and repair (Yang et al. 2014) and slr0151 inactivation results in impaired TM morphology (Rast et al. 2016). Unlike the other two TPR proteins PratA and Pitt, and probably consistent with its wider distribution both within convergence zones and throughout the TMs (Rast et al., 2016), Slr0151 is quantified in our analysis at 4450–7900 cpc (Fig. 4b). Furthermore, there is evidence that Slr0151 has a greater range of interaction partners than PratA and Pitt including PSII subunits PsbA/D1 and PsbC/CP43 (Yang et al. 2014), and is involved in the modulation of Fd-5 phosphorylation (Angeleri et al. 2018).

Pam68, Ycf48 and RubA The Pam68 assembly factor, first characterized in Arabidopsis as TM-intrinsic, was identified by homology with Sll0933 in *Synechocystis* (Armbruster et al. 2010). Using FLAG-tagged Pam68, Bučinská et al. (2018) co-isolated a complex containing PsbB/CP47 as the only PSII subunit represented, alongside YidC, SecY and several riboproteins. These associations reveal that the probable function of Pam68 is facilitating the co-translational insertion of PsbB/CP47 into the TM and possibly

also the correct apoprotein configuration for the delivery of Chl (Bučinská et al. 2018). Co-isolating with Pam68 in IP analysis is the lumenal protein Ycf48 (Rengstl et al. 2013; Bučinská et al. 2018). Ycf48 is homologous with Arabidopsis HCF136 (Meurer et al. 1998) and was shown to be essential for the accumulation of PsbB/CP47 and PsbC/CP43 in the TM (Rengstl et al. 2013). It has been proposed that Ycf48 may, like Pam68, facilitate co-translational Chl delivery to nascent apoproteins (Crawford et al. 2016). We quantified Pam68 and Ycf48 at 1250–1600 and 3600–5150 cpc, respectively (Fig. 4b). We suggest that Ycf48 is approximately threefold more abundant than Pam68 because it associates with a greater number of precursor modules: CP47, CP43 (Rengstl et al. 2013), D1 and RCII (Yu et al. 2018). Another component of the D1 assembly complex, with evidence of a direct association with Ycf48, is RubA (Slr2033; Kiss et al. 2019), quantified here at 2850–7150 cpc.

Psb27 and Psb28 Analysis of intermediates in PSII biogenesis by immunoblotting identified Psb27 as a component of assembly modules containing PsbC/CP43 (Komenda et al. 2012; Fig. 4b) and recent structural analyses by cryo-EM revealed not only docking sites on PsbC/CP43 (Zabret et al. 2021) but also the induction of conformational changes in PsbB/CP47 and PsbD/D2 (Huang et al. 2021). According to IP analysis, Psb28 co-isolates with the RC47 assembly module (Bečková et al. 2017), docking with both PsbA/D1 and PsbD/D2 subunits, where it induces temporary conformational changes that may protect nascent PSII from photodamage until the Mn_4CaO_5 cluster is assembled and water oxidation activated (Zabret et al. 2021). Psb27 and Psb28 (Sll1398) were quantified as relatively high abundance assembly factors at 3500–60,500 and 28,000–100,000 cpc respectively, reflecting their participation in interactions with multiple PSII assembly intermediates (Komenda et al. 2012; Bečková et al. 2017; Pascual-Aznar et al. 2021). A second isoform of Psb28 encoded by slr1739 (Boehm et al. 2012a) and proposed to have a divergent function (Bečková et al. 2017) was identified with only two peptides in the label-free DDA analysis (Supplementary Data Set S4) and therefore not validated for quantification.

Thylakoid membrane biogenesis and photosystem I assembly

It may be argued that CurT facilitates the accumulation of PSII indirectly via its role in inducing the correct TM architecture and that this activity of CurT also provides the TM environment for PSI biogenesis. Unexpectedly however, inactivation of *curT* has been shown to have no effect on PSI abundance (Heinz et al. 2016), highlighting a link

between TM biogenesis and PSI assembly via an alternative mechanism.

VIPP1 In addition, referred to as IM30, VIPP1 was first identified in chloroplasts as essential for TM biogenesis (Kroll et al. 2001), with membrane insertion of PsaA and PsaB compromised in a Δ*vipp1* strain of *Synechococcus* sp. PCC 7002. This evidence suggests that VIPP1 is actually functional in PSI biogenesis and that the presence of PSI, with CurT, is required for the formation of normal TM architecture (Zhang et al. 2014). Structural characterization has established that VIPP1 binds to the membrane surface as homo-oligomers of > 1 MDa (Aseeva et al. 2004) forming stacked rings that induce curvature of the membrane into a central hydrophobic channel (Gupta et al. 2021). In view of this MDa size, the 40,500–45,000 cpc abundance determined in this analysis (Fig. 4c) suggests the actual number of functional VIPP1 units within the TM may be only 1000–1200. Unlike CurT, which may be maintained at high abundance because its membrane curvature activity is a constant requirement over the entire TM, VIPP1 is proposed to have a localized function at convergence zones where it may participate in lipid transfer between the CM and nascent TM (Gupta et al. 2021).

Ycf3, Ycf37 and Ycf4 Although PSI assembly occurs so rapidly that the isolation of intermediate subcomplexes has proved challenging (Schöttler et al. 2011), several assembly factors have emerged from the investigation of mutants with defective PSI accumulation (Wilde et al. 1995; Boudreau et al. 1997; Bartsevich and Pakrasi 1997; Wilde et al. 2001).

Ycf3 is a hydrophilic TPR protein that was found to co-isolate in IP analysis with PsaA and PsaD on the cytoplasmic surface of the TM (Naver et al. 2001). A similar strategy demonstrated the association of subunits PsaA-D with Ycf37, a TPR protein anchored in the TM by one TMH, also on the cytoplasmic surface. Furthermore, Ycf37 co-migrated with PSI(1), not PSI(3) after sucrose gradient centrifugation, indicating its possible role in PSI trimerization (Dühring et al. 2006). Ycf3 and Ycf37 are quantified here at comparable abundance levels: 2950–4750 and 1750–5300 cpc respectively (Fig. 4c), suggesting that these proteins may have similar stoichiometric relationships with nascent PSI complexes. Their approximate 20-fold lower abundance than the cellular PSI population (86,000–118,500 cpc; Fig. 1a) supports the view that Ycf3 and Ycf37 operate as chaperones, interacting only transiently with their respective binding partners.

The use of TAP-tagged Ycf4 has revealed interactions with six subunits: PsaA-PsaF, with stability dependent on bound PsaF (Ozawa et al. 2009). In a model proposed by Nellaepalli et al. (2021), Ycf3 is the first to bind to a newly synthesized PsaA/B heterodimer, followed by Ycf4 which stabilizes the complex as more subunits join, followed by Ycf37. Ycf4 is quantified at 6800–14,000 cpc (Fig. 4c), almost twofold higher than Ycf3 and Ycf37. This 1:1:2 stoichiometry for Ycf3:Ycf37:Ycf4 may be explained if Ycf4 is active as a dimer.

FtsH proteases

The PsbA/D1 subunit of PSII is highly susceptible to photo-oxidative damage as part of its normal function (Adir et al. 2003). To maintain continuity of PSII activity and enable acclimation to changing illumination, a repair mechanism has evolved in oxygenic phototrophs (Nixon et al. 2005). Four homologous, membrane intrinsic, ATP-dependent Zn-metalloproteases encoded by *ftsH1-4* are involved in PSII repair and a wide range of other cellular processes. Their functional diversity is based on the assembly of different combinations of both homo- and hetero-oligomeric complexes (Mann et al. 2000; Boehm et al. 2012b). All four were quantified in the analysis reported here, ensuring that only unique proteotypic tryptic peptides were used. The *Synechocystis* FtsH proteases all have similar sequence identities (41–47%) to the single FtsH occurring in *E. coli*, with a reported abundance of 660 cpc (Wiśniewskia and Rakus, 2014). This level is in close agreement with our determination of FtsH1 at < 1000 cpc (Fig. 4d), suggesting that FtsH1 is the basic isoform (Bittner et al. 2017). The 3–sixfold higher levels of FtsH2, FtsH3 and FtsH4 at 1800–5150, 2400–3000 and 2800–5950 cpc, respectively, may reflect functions that extend beyond the remit of a basic FtsH protease, with a greater number of protein targets. Both FtsH2 and FtsH3 are functional in the degradation of photodamaged PsbA/D1 (Silva et al. 2003; Komenda et al. 2006), specifically as an FtsH2/3 complex (Boehm et al. 2012b). An FtsH1/3 complex plays a role in the regulation of gene expression in acclimation to nutrient stress (Krynická et al. 2014; 2019).

Conclusions

We employed four mass spectrometry-based quantification methods, which revealed the cellular levels of 97 proteins involved in photosynthesis, the biosynthesis of carotenoid, chlorophyll and bilin pigments, membrane assembly, the light reactions of photosynthesis, fixation of carbon dioxide and nitrogen, hydrogen, and sulfur metabolism. Figure 5 summarizes the cellular locations and associations of these proteins, also indicating that regulatory and biosynthetic components are generally less abundant than those involved in bioenergetic reactions. We also found disparities in the abundances of subunits relative to their stoichiometries apparent in high-resolution structures, as expected given that both complete complexes
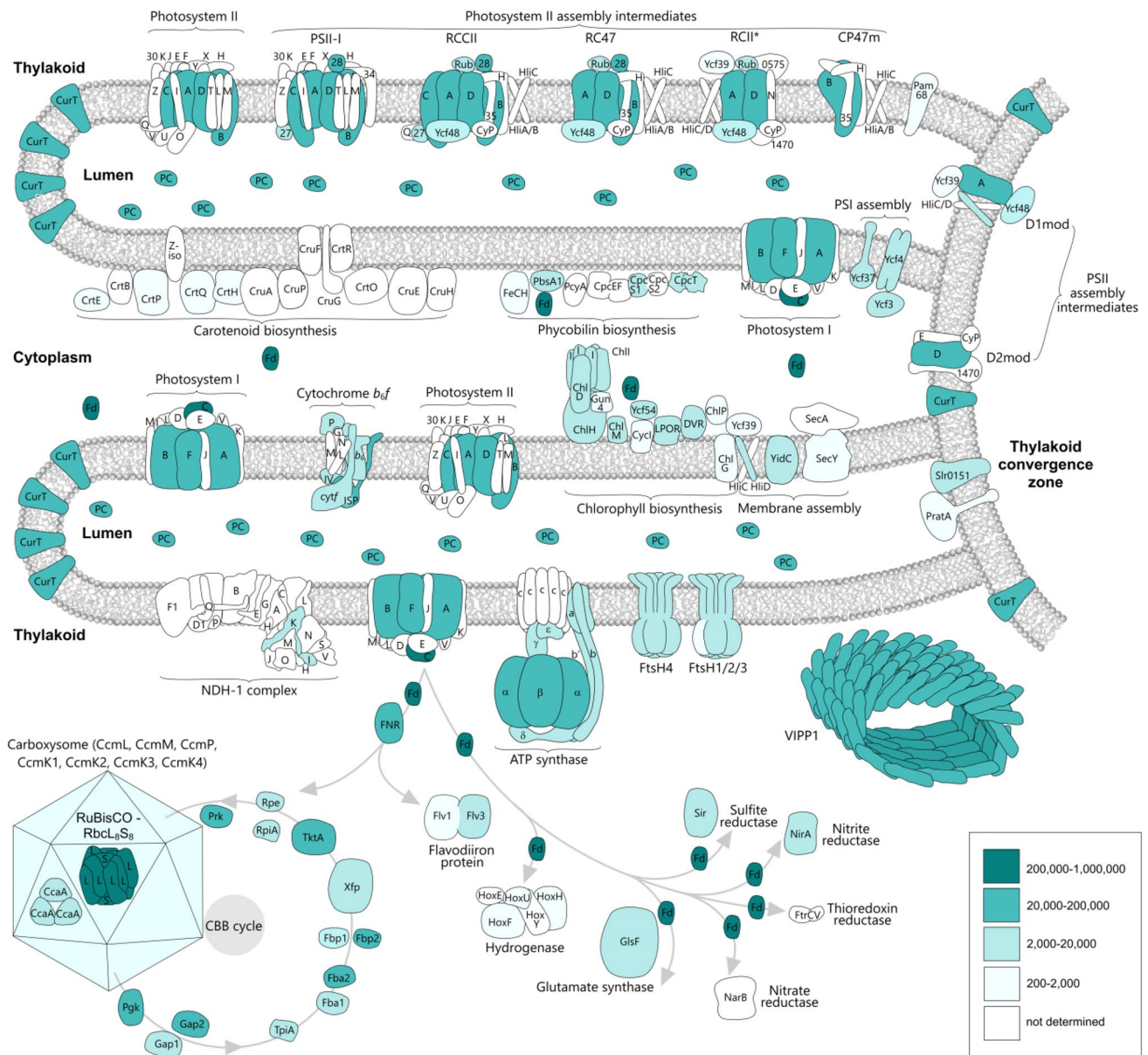
Fig. 5 Diagrammatic summary of the proteins quantified in this study, showing the range of biological processes, such as biosynthetic and assembly pathways, covered by the quantitative mass spectrometry analysis. Abbreviations are defined in Figs. 1, 2,3, 4. Proteins and subunits of complexes that have been quantified are colored in blue and shaded according their abundance levels; those not quantified are in white. Complexes such as photosystem I, photosystem II and cytochrome b_6f are drawn as monomers for simplicity. Thylakoids are drawn as elongated tubular structures, which converge on a thylakoid convergence zone that appears to connect plasma and thylakoid membranes (Stengel et al. 2012; Heinz et al. 2016). The photosystem II assembly intermediates are based on those in Konert et al. (2022) and Rahimzadeh-Karvansara (2022), with the exception of the PSII-I assembly complex, the structure of which was determined by Zabret et al. (2021)

and assembly intermediates would contribute to the analysis. Furthermore, we were able to calculate cellular levels for some large complexes such as photosystems, assemblies such as carboxysomes and VIPP1 oligomers, and hexameric FtsH Zn-metalloproteinases.

Our quantitative proteomic baseline for wild-type *Synechocystis* enhances our understanding of this model organism

and will be a valuable resource for the photosynthesis community, as well as forming the basis for synthetic biology projects aimed at manipulating biosynthetic, metabolic and energy-transducing pathways. *Synechocystis* is an important model organism for engineering photosynthetic metabolism and knowing the numbers of the essential components will inform attempts to use this bacterium as a chassis for using

sunlight, CO_2 and water to produce valuable metabolites and increased biomass. While the focus of this study has been on the 97 proteins described, cellular levels of 1081 proteins are also presented.

Declarations

References

Mills LA, McCormick AJ, Lea-Smith DJ (2020) Current knowledge and recent advances in understanding metabolism of the model cyanobacterium *Synechocystis* sp. PCC 6803. Bioscience rep 40: BSR20193325. https://doi.org/10.1042/BSR20193325

Adams NBP, Reid JD (2013) The allosteric role of the AAA+ domain of ChlD protein from the magnesium chelatase of *Synechocystis* species PCC 6803. J Biol Chem 288:28727–28732. https://doi.org/10.1074/jbc.M113.477943

Adams NBP, Vasilev C, Brindley AA, Hunter CN (2016) Nanomechanical and thermophoretic analyses of the nucleotide-dependent interactions between the AAA+ subunits of magnesium chelatase.

J Am Chem Soc 138:6591–6597. https://doi.org/10.1021/jacs.6b02827

Adams NBP, Bisson C, Brindley AA, Farmer DA, Davison PA, Reid JD, Hunter CN (2020) The active site of magnesium chelatase. Nat Plants 6:1491–1502. https://doi.org/10.1038/s41477-020-00806-9

Adir N, Zer H, Shochat S, Ohad I (2003) Photoinhibition – a historical perspective. Photosynth Res 76:343–370. https://doi.org/10.1023/A:1024969518145

Al Shweiki MHDR, Mönchgesang S, Majovsky P, Thieme D, Trutschel D, Hoehenwarter W (2017) Assessment of label-free quantification in discovery proteomics and impact of technological factors and natural variability of protein abundance. J Proteome Res 16:1410–1424. https://doi.org/10.1021/acs.jproteome.6b00645

Aldridge C, Spence E, Kirkilionis MA, Frigerio L, Robinson C (2008) Tat-dependent targeting of Rieske iron-sulphur proteins to both the plasma and thylakoid membranes in the cyanobacterium *Synechocystis* PCC6803. Mol Microbiol 70:140–150. https://doi.org/10.1111/j.1365-2958.2008.06401.x

Allahverdiyeva Y, Ermakova M, Eisenhut M, Zhang P, Richaud P, Hagemann M, Cournac L, Aro EM (2011) Interplay between flavodiiron proteins and photorespiration in *Synechocystis* sp. PCC 6803. J Biol Chem 286:24007–24014. https://doi.org/10.1074/jbc.M111.223289

Allen MD, Kropat J, Merchant SS (2008) Regulation and localization of isoforms of the aerobic oxidative cyclase in *Chlamydomonas reinhardtii*. Photochem Photobiol 84:1336–1342. https://doi.org/10.1111/j.1751-1097.2008.00440.x

Anderson LK, Toole CM (1998) A model for early events in the assembly pathway of cyanobacterial phycobilisomes. Mol Microbiol 30:467–474. https://doi.org/10.1046/j.1365-2958.1998.01081.x

Andersson I, Backlund A (2008) Structure and function of Rubisco. Plant Physiol Biochem 46:275–291. https://doi.org/10.1016/j.plaphy.2008.01.001

Angeleri M, Zorina A, Aro EM, Battchikova N (2018) Interplay of SpkG kinase and the Slr0151 protein in the phosphorylation of ferredoxin 5 in Synechocystis sp. strain PCC 6803. FEBS Lett 592:411–421. https://doi.org/10.1002/1873-3468.12970

Angeleri M, Muth-Pawlak D, Wilde A, Aro EM, Battchikova N (2019) Global proteome response of *Synechocystis* 6803 to extreme copper environments applied to control the activity of the inducible *petJ* promoter. J Appl Microbiol 126:826–841. https://doi.org/10.1111/jam.14182

Arike L, Valgepea K, Peil L, Nahku R, Adamberg K, Vilu R (2013) Comparison and applications of label-free absolute proteome quantification methods on *Escherichia coli*. J Proteomics 75:5437–5448. https://doi.org/10.1016/j.jprot.2012.06.020

Armbruster U, Zühlke J, Rengstl B, Kreller R, Makarenko E, Rühle T, Schünemann D, Jahns P, Weisshaar B, Nickelsen J, Leister D (2010) The Arabidopsis thylakoid protein PAM68 is required for efficient D1 biogenesis and photosystem II assembly. Plant Cell 22:3439–3460. https://doi.org/10.1105/tpc.110.077453

Aseeva E, Ossenbühl F, Eichacker LA, Wanner G, Soll J, Vothknecht UC (2004) Complex formation of Vipp1 depends on its α-helical PspA-like domain. J Biol Chem 279:35535–35541. https://doi.org/10.1074/jbc.M401750200

Badger MR, Hanson D, Price GD (2002) Evolution and diversity of CO_2 concentrating mechanisms in cyanobacteria. Funct Plant Biol 29:161–173. https://doi.org/10.1071/PP01213

Baebprasert W, Jantaro S, Khetkorn W, Lindblad P, Incharoensakdi A (2011) Increased H_2 production in the cyanobacterium *Synechocystis* sp. strain PCC 6803 by redirecting the electron supply via genetic engineering of the nitrate assimilation pathway. Metabolic Eng 13:610–616. https://doi.org/10.1016/j.ymben.2011.07.004

Baers LL, Breckels LM, Mills LA, Gatto L, Deery MJ, Stevens TJ, Howe CJ, Lilley KS, Lea-Smith DJ (2019) Proteome mapping of a cyanobacterium reveals distinct compartment organization and cell-dispersed metabolism. Plant Physiol 181:1721–1738. https://doi.org/10.1104/pp.19.00897

Bartsevich VV, Pakrasi HB (1997) Molecular identification of a novel protein that regulates biogenesis of photosystem I, a membrane protein complex. J Biol Chem 272:6382–6387. https://doi.org/10.1074/jbc.272.10.6382

Battchikova N, Muth-Pawlak D, Aro E-M (2018) Proteomics of cyanobacteria: current horizons. Curr Opin Biotechnol 54:65–71. https://doi.org/10.1016/j.copbio.2018.02.012

Bečková M, Gardian Z, Yu J, Konik P, Nixon PJ, Komenda J (2017) Association of Psb28 and Psb27 proteins with PSII-PSI super-complexes upon exposure of *Synechocystis* sp. PCC 6803 to high light. Mol Plant 10:62–72. https://doi.org/10.1016/j.molp.2016.08.001

Bečková M, Sobotka R, Komenda J (2022) Photosystem II antenna modules CP43 and CP47 do not form a stable 'no reaction centre complex' in the cyanobacterium *Synechocystis* sp. PCC 6803. Photosynth Res 11:1–9. https://doi.org/10.1007/s11120-022-00896-w

Berner RA, Petsch ST, Lake JA, Beerling DJ, Popp BN, Lane RS, Laws EA, Westley MB, Cassar N, Woodward FI, Quick WP (2000) Isotope fractionation and atmospheric oxygen: implications for phanerozoic O_2 evolution. Science 287:1630–1633. https://doi.org/10.1126/science.287.5458.1630

Bittner LM, Arends J, Narberhaus F (2017) When how and why? Regulated proteolysis by the essential FtsH protease in *Escherichia coli*. Biol Chem 398(5–6):625–635. https://doi.org/10.1515/hsz-2016-0302

Boehm M, Yu J, Reisinger V, Beckova M, Eichacker LA, Schlodder E, Komenda J, Nixon PJ (2012a) Subunit composition of CP43-less photosystem II complexes of *Synechocystis* sp. PCC 6803: implications for the assembly and repair of photosystem II. Phil Trans Roy Soc B: Biol Sci 367:3444–3454. https://doi.org/10.1098/rstb.2012.0066

Boehm M, Yu J, Krynicka V, Barker M, Tichy M, Komenda J, Nixon PJ, Nield J (2012b) Subunit organization of a *Synechocystis* hetero-oligomeric thylakoid FtsH complex involved in photosystem II repair. Plant Cell 24:3669–3683. https://doi.org/10.1105/tpc.112.100891

Bollivar D, Braumann I, Berendt K, Gough SP, Hansson M (2014) The Ycf54 protein is part of the membrane component of Mg-protoporphyrin IX monomethyl ester cyclase from barley (*Hordeum vulgare* L). FEBS J 281:2377–2386. https://doi.org/10.1111/febs.12790

Boudreau E, Takahashi Y, Lemieux C, Turmel M, Rochaix J-D (1997) The chloroplast *ycf3* and *ycf4* open reading frames of *Chlamydomonas reinhardtii* are required for the accumulation of the photosystem I complex. EMBO J 16:6095–6104. https://doi.org/10.1093/emboj/16.20.6095

Brownridge P, Lawless C, Payapilly AB, Lanthaler K, Holman SW, Harman VM, Grant CM, Beynon RJ, Hubbard SJ (2013) Quantitative analysis of chaperone network throughput in budding yeast. Proteomics 13:1276–1291. https://doi.org/10.1002/pmic.201200412

Brun V, Dupuis A, Adrait A, Marcellin M, Thomas D, Court M, Vandenesch F, Garin J (2007) Isotope-labeled protein standards: toward absolute quantitative proteomics. Mol Cell Proteomics 6:2139–2149. https://doi.org/10.1074/mcp.M700163-MCP200

Bryant DA, Hunter CN, Warren MJ (2020) Biosynthesis of the modified tetrapyrroles — the pigments of life. J Biol Chem 295:6888–6925. https://doi.org/10.1074/jbc.REV120.006194

Bučinská L, Kiss É, Koník P, Knoppová J, Komend J, Sobotka R (2018) The ribosome-bound protein Pam68 promotes insertion of chlorophyll into the CP47 subunit of photosystem II. Plant Physiol 176:2931–2942. https://doi.org/10.1104/pp.18.00061

Cai F, Menon BB, Cannon GC, Curry KJ, Shively JM, Heinhorst S (2009) The pentameric vertex proteins are necessary for the icosahedral carboxysome shell to function as a CO_2 leakage barrier. PLoS ONE 4:e7521. https://doi.org/10.1371/journal.pone.0007521

Cai F, Sutter M, Cameron JC, Stanley DN, Kinney JN, Kerfeld CA (2013) The structure of CcmP, a tandem bacterial microcompartment domain protein from the β-carboxysome, forms a subcompartment within a microcompartment. J Biol Chem 288:16055–16063. https://doi.org/10.1074/jbc.M113.456897

Cameron JC, Wilson SC, Bernstein SL, Kerfeld CA (2013) Biogenesis of a bacterial organelle: the carboxysome assembly pathway. Cell 155:1131–1140. https://doi.org/10.1016/j.cell.2013.10.044

Canniffe DP, Hitchcock A (2021) Photosynthesis Carotenoids in Photosynthesis: Structure and Biosynthesis. In: Jez J (ed) Encyclopedia of biological chemistry III. Elsevier, Oxford

Canniffe DP, Chidgey JW, Hunter CN (2014) Elucidation of the preferred routes of C8-vinyl reduction in chlorophyll and bacteriochlorophyll biosynthesis. Biochem J 462:433–440. https://doi.org/10.1042/BJ20140163

Carroll KM, Simpson DM, Eyers CE, Knight CG, Brownridge P, Dunn WB, Winder CL, Lanthaler K, Pir P, Malys N, Kell DB, Oliver SG, Gaskell SJ, Beynon RJ (2011) Absolute quantification of the glycolytic pathway in yeast: deployment of a complete QconCAT approach. Mol Cell Proteomics 10(M111):007633. https://doi.org/10.1074/mcp.M111.007633

Cartron ML, Olsen JD, Sener M, Jackson PJ, Brindley AA, Qian P, Dickman MJ, Leggett GJ, Schulten K, Hunter CN (2014) Integration of energy and electron transfer processes in the photosynthetic membrane of *Rhodobacter sphaeroides*. Biochim Biophys Acta Bioenerg 1837:1769–1780. https://doi.org/10.1016/j.bbabio.2014.02.003

Casella S, Huang F, Mason D, Zhao GY, Johnson GN, Mullineaux CW, Liu LN (2017) Dissecting the native architecture and dynamics of cyanobacterial photosynthetic machinery. Mol Plant 10:1434–1448. https://doi.org/10.1016/j.molp.2017.09.019

Cassier-Chauvat C, Chauvat F (2014) Function and regulation of ferredoxins in the cyanobacterium *Synechocystis* PCC 6803: recent advances. Life 4:666–680. https://doi.org/10.3390/life4040666

Chambers MC, Maclean B, Burke R et al (2012) A cross-platform toolkit for mass spectrometry and proteomics. Nat Biotechnol 30:918–920. https://doi.org/10.1038/nbt.2377

Chang C, Gao Z, Ying W, Fu Y, Zhao Y, Wu S, Li M, Wang G, Qian X, Zhu Y, He F (2018) LFAQ: Toward unbiased label-free absolute protein quantification by predicting peptide quantitative factors. Anal Chem 91:1335–1343. https://doi.org/10.1021/acs.analchem.8b03267

Chen Y, Li F, Wurtzel ET (2010) Isolation and characterization of the *Z-ISO* gene encoding a missing component of carotenoid biosynthesis in plants. Plant Physiol 153:66–79. https://doi.org/10.1104/pp.110.153916

Chen GE, Adams NBP, Jackson PJ, Dickman MJ, Hunter CN (2021) How the O_2-dependent Mg-protoporphyrin monomethyl ester cyclase forms the fifth ring of chlorophylls. Nat Plants 7:365–375. https://doi.org/10.1038/s41477-021-00876-3

Chidgey JW, Linhartová M, Komenda J, Jackson PJ, Dickman MJ, Canniffe DP, Koník P, Pilný J, Hunter CN, Sobotka RA (2014) A cyanobacterial chlorophyll synthase-HliD complex associates with the Ycf39 protein and the YidC/Alb3 insertase. Plant Cell 26:1267–1279. https://doi.org/10.1105/tpc.114.124495

Cogdell RJ, Howard TD, Bittl R, Schlodder E, Geisenheimer I, Lubitz W (2000) How carotenoids protect bacterial photosynthesis. Philos Trans R Soc Lond B Biol Sci 355:1345–1349. https://doi.org/10.1098/rstb.2000.0696

Cole J, Hanson EJ, James DC, Dockrell DH, Dickman MJ (2019) Comparison of data-acquisition methods for the identification and quantification of histone post-translational modifications on a Q Exactive HF hybrid quadrupole Orbitrap mass spectrometer. Rapid Commun Mass Spectrom 33:897–906. https://doi.org/10.1002/rcm.8401

Çoruh O, Frank A, Tanaka H, Kawamoto A, El-Mohsnawy E, Kato T, Namba K, Gerle C, Nowaczyk MM, Kurisu G (2021) Cryo-EM structure of a functional monomeric Photosystem I from *Thermosynechococcus elongatus* reveals red chlorophyll cluster. Commun Biol 4:1–16. https://doi.org/10.1038/s42003-021-01808-9

Cot SS, So AK, Espie GS (2008) A multiprotein bicarbonate dehydration complex essential to carboxysome function in cyanobacteria. J Bact 190:936–945. https://doi.org/10.1128/JB.01283-07

Cox J, Mann M (2008) MaxQuant enables high peptide identification rates, individualized ppb-range mass accuracies and proteome-wide protein quantification. Nat Biotechnol 26:1367–1372. https://doi.org/10.1038/nbt.1511

Crawford TS, Eaton-Rye JJ, Summerfield TC (2016) Mutation of gly195 of the chlH subunit of Mg-chelatase reduces chlorophyll and further disrupts PS II assembly in a Ycf48-deficient strain of *Synechocystis* sp. PCC 6803. Front Plant Sci. https://doi.org/10.3389/fpls.2016.01060

Dann M, Leister D (2017) Enhancing (crop) plant photosynthesis by introducing novel genetic diversity. Phil Trans R Soc B 372:20160380. https://doi.org/10.1098/rstb.2016.0380

Dann M, Ortiz EM, Thomas M, Guljamow A, Lehmann M, Schaefer H, Leister D (2021) Enhancing photosynthesis at high light levels by adaptive laboratory evolution. Nat Plants 7:681–695. https://doi.org/10.1038/s41477-021-00904-2

Davison PA, Hunter CN (2011) Abolition of magnesium chelatase activity by the *gun5* mutation and reversal by Gun4. FEBS Lett 585:183–186. https://doi.org/10.1016/j.febslet.2010.11.037

Davison PA, Schubert HL, Reid JD, Iorg CD, Heroux A, Hill CP, Hunter CN (2005) Structural and biochemical characterization of Gun4 suggests a mechanism for its role in chlorophyll biosynthesis. Biochem 44:7603–7612. https://doi.org/10.1021/bi050240x

Deckers-Hebestreit G (2013) Assembly of the *Escherichia coli* FoF1 ATP synthase involves distinct subcomplex formation. Biochem Soc Trans 41:1288–1293. https://doi.org/10.1042/BST20130096

Domínguez-Martín MA, Sauer PV, Kirst H et al (2022) Structures of a phycobilisome in light-harvesting and photoprotected states. Nature 609:835–845. https://doi.org/10.1038/s41586-022-05156-4

Dühring U, Irrgang KD, Lünser K, Kehr J, Wilde A (2006) Analysis of photosynthetic complexes from a cyanobacterial *ycf37* mutant. Biochim Biophys Acta Bioenerg 1757:3–11. https://doi.org/10.1016/j.bbabio.2005.11.001

Fabre B, Lambour T, Bouyssié D, Menneteau T, Monsarrat B, Burlet-Schiltz O, Bousquet-Dubouch M-P (2014) Comparison of label-free quantification methods for the determination of protein complexes subunits stoichiometry. EuPA Open Proteom 4:82–86. https://doi.org/10.1016/j.euprot.2014.06.001

Fairchild CD, Zhao J, Zhou J, Colson SE, Bryant DA, Glazer AN (1992) Phycocyanin alpha-subunit phycocyanobilin lyase. Proc Natl Acad Sci USA 89:7017–7021. https://doi.org/10.1073/pnas.89.15.7017

Farmer DA, Brindley AA, Hitchcock A, Jackson PJ, Johnson B, Dickman MJ, Hunter CN, Reid JD, Adams N (2019) The ChlD subunit links the motor and porphyrin binding subunits of magnesium chelatase. Biochem J 476:1875–1887. https://doi.org/10.1042/BCJ20190095

Faulkner M, Rodriguez-Ramos J, Dykes GF, Owen SV, Casella S, Simpson DM, Beynon RJ, Liu LN (2017) Direct characterization of the native structure and mechanics of cyanobacterial carboxysomes. Nanoscale 9:10662–10673. https://doi.org/10.1039/c7nr02524f

Fernández-González B, Sandmann G, Vioque A (1997) A new type of asymmetrically acting beta-carotene ketolase is required for the synthesis of echinenone in the cyanobacterium *Synechocystis* sp. PCC 6803. J Biol Chem 272:9728–9733. https://doi.org/10.1074/jbc.272.15.9728

Ferreira KN, Iverson TM, Maghlaoui K, Barber J, Iwata S (2004) Architecture of the photosynthetic oxygen-evolving center. Science 303:1831–1838. https://doi.org/10.1126/science.1093087

Field CB, Behrenfeld MJ, Randerson JT, Falkowski P (1998) Primary Production of the biosphere: integrating terrestrial and oceanic components. Science 10:237–240. https://doi.org/10.1126/science.281.5374.237

Flamholz AI, Prywes N, Moran U, Davidi D, Bar-On YM, Oltrogge LM, Alves R, Savage D, Milo R (2019) Revisiting trade-offs between Rubisco kinetic parameters. Biochemistry 58:3365–3376. https://doi.org/10.1021/acs.biochem.9b00237

Flannery SE, Hepworth C, Wood WH, Pastorelli F, Hunter CN, Dickman MJ, Jackson PJ, Johnson MP (2021) Developmental acclimation of the thylakoid proteome to light intensity in *Arabidopsis*. Plant J 105:223–244. https://doi.org/10.1111/tpj.15053

Fodje MN, Hansson A, Hansson M, Olsen JG, Gough S, Willows RD, Al Karadaghi S (2001) Interplay between an AAA module and an integrin I domain may regulate the function of magnesium chelatase. J Mol Biol 311:111–122. https://doi.org/10.1006/jmbi.2001.4834

Fraser JM, Tulk SE, Jeans JA, Campbell DA, Bibby TS, Cockshutt AM (2013) Photophysiological and photosynthetic complex changes during iron starvation in *Synechocystis* sp PCC 6803 and *Synechococcus elongatus* PCC 7942. PLoS ONE 8:e59861. https://doi.org/10.1371/journal.pone.0059861

Fujita Y, Murakami A (1987) Regulation of electron transport composition in cyanobacterial photosynthetic system: stoichiometry among photosystem I and II complexes and their light-harvesting antennae and cytochrome b_6f complex. Plant Cell Physiol 28:1547–1553. https://doi.org/10.1093/oxfordjournals.pcp.a077449

Fulda S, Huang F, Nilsson F, Hagemann M, Norling B (2000) Proteomics of *Synechocystis* sp strain PCC 6803: identification of periplasmic proteins in cells grown at low and high salt concentrations. Eur J Biochem 267:5900–5907. https://doi.org/10.1046/j.1432-1327.2000.01642.x

Gao L, Wang J, Ge H, Fang L, Zhang Y, Huang X, Wang Y (2015) Toward the complete proteome of *Synechocystis* sp PCC 6803. Photosynth Res 126:203–219. https://doi.org/10.1007/s11120-015-0140-y

Gao J, Wang H, Yuan Q, Feng Y (2018) Structure and function of the photosystem supercomplexes. Front Plant Sci 9:357. https://doi.org/10.3389/fpls.2018.00357

Gao Y-S, Wang Y-L, Wang X, Liu L (2020) Hexameric structure of the ATPase motor subunit of magnesium chelatase in chlorophyll biosynthesis. Protein Sci 29:1026–1032. https://doi.org/10.1002/pro.3816

García-Cañas R, Giner-Lamia J, Florencio FJ, López-Maury L (2021) A protease-mediated mechanism regulates the cytochrome c_6/plastocyanin switch in *Synechocystis* sp PCC 6803. Proc Natl Acad Sci USA 118:e2017898118. https://doi.org/10.1073/pnas.2017898118

Gaubier P, Wu HJ, Laudie´ M, Delseny M, Grellet, F, (1995) A chlorophyll synthetase gene from *Arabidopsis thaliana*. Mol Gen Genet 249:58–64. https://doi.org/10.1007/BF00290236

Gisriel C, Coe J, Letrun R et al (2019) Membrane protein megahertz crystallography at the European XFEL. Nat Commun 10:1–11. https://doi.org/10.1038/s41467-019-12955-3

Gisriel CJ, Wang J, Liu J, Flesher DA, Reiss KM, Huang HL, Yang KR, Armstrong WH, Gunner MR, Batista VS, Debus RJ (2022) High-resolution cryo-electron microscopy structure of photosystem II from the mesophilic cyanobacterium, Synechocystis sp PCC 6803. Proc Natl Acad of Sci USA. https://doi.org/10.1073/pnas.2116765118

Graham JE, Bryant DA (2008) The biosynthetic pathway for synechoxanthin, an aromatic carotenoid synthesized by the euryhaline, unicellular cyanobacterium *Synechococcus* sp. strain PCC 7002. J Bacteriol 190:7966–7974. https://doi.org/10.1128/JB.00985-08

Graham JE, Bryant DA (2009) The biosynthetic pathway for myxol-2' fucoside (myxoxanthophyll) in the cyanobacterium *Synechococcus* sp. strain PCC 7002. J Bacteriol 191:3292–3300. https://doi.org/10.1128/JB.00050-09

Graham JE, Lecomte JT, Bryant DA (2008) Synechoxanthin, an aromatic C40 xanthophyll that is a major carotenoid in the cyanobacterium *Synechococcus* sp. PCC 7002. J Nat Prod 71:1647–1650. https://doi.org/10.1021/np800310b

Guo H, Suzuki T, Rubinstein JL (2019) Structure of a bacterial ATP synthase. Elife 8:e43128. https://doi.org/10.7554/eLife.43128

Gupta TK, Klumpe S, Gries K et al (2021) Structural basis for VIPP1 oligomerization and maintenance of thylakoid membrane integrity. Cell 184:3643–3659. https://doi.org/10.1016/j.cell.2021.05.011

Hammel A, Zimmer D, Sommer F, Mühlhaus T, Schroda M (2018) Absolute quantification of major photosynthetic protein complexes in *Chlamydomonas reinhardtii* using quantification concatamers (QconCATs). Front Plant Sci 9:1265. https://doi.org/10.3389/fpls.2018.01265

Hayes JM, Mantle TJ (2009) The effect of pH on the initial rate kinetics of the dimeric biliverdin-IXα reductase from the cyanobacterium *Synechocystis* PCC6803. FEBS J 276:4414–4425. https://doi.org/10.1111/j.1742-4658.2009.07149.x

Heinz S, Liauw P, Nickelsen J, Nowaczyk M (2016) Analysis of photosystem II biogenesis in cyanobacteria. Biochim Biophys Acta Bioenerg 1857:274–287. https://doi.org/10.1016/j.bbabio.2015.11.007

Herbst J, Girke A, Hajirezaei MR, Hanke G, Grimm B (2018) Potential roles of YCF54 and ferredoxin-NADPH reductase for magnesium protoporphyrin monomethylester cyclase. Plant J 94:485–496. https://doi.org/10.1111/tpj.13869

Heyes DJ, Heathcote P, Rigby SEJ, Palacios MA, van Grondelle R, Hunter CN (2006) The first catalytic step of the light-driven enzyme protochlorophyllide oxidoreductase proceeds via a charge transfer complex. J Biol Chem 281:26847–26853. https://doi.org/10.1074/jbc.M602943200

Hihara Y, Sonoike K, Ikeuchi M (1998) A novel gene, *pmgA*, specifically regulates photosystem stoichiometry in the cyanobacterium *Synechocystis* species PCC 6803 in response to high light. Plant Physiol 117:1205–1216. https://doi.org/10.1104/pp.117.4.1205

Hill NC, Tay JW, Altus S, Bortz DM, Cameron JC (2020) Life cycle of a cyanobacterial carboxysome. Sci Adv. https://doi.org/10.1126/sciadv.aba1269

Hing NY, Liang F, Lindblad P, Morgan JA (2019) Combining isotopically non-stationary metabolic flux analysis with proteomics to unravel the regulation of the Calvin-Benson-Bassham cycle in *Synechocystis* sp. PCC 6803. Metabolic Eng 56:77–84. https://doi.org/10.1016/j.ymben.2019.08.014

Hisashi H, Yokono M, Tanaka R, Tanaka A (2008) Identification of a novel vinyl reductase gene essential for the biosynthesis of monovinyl chlorophyll in *Synechocystis* sp PCC 6803. J Biol Chem 283:9002–9011. https://doi.org/10.1074/jbc.M708369200

Hollingshead S, Kopečná J, Jackson PJ, Canniffe DP, Davison PA, Dickman MJ, Sobotka R, Hunter CN (2012) Conserved chloroplast open-reading frame *ycf54* is required for activity of the magnesium protoporphyrin monomethylester oxidative cyclase in *Synechocystis* PCC 6803. J Biol Chem 287:27823–27833. https://doi.org/10.1074/jbc.M112.352526

Hollingshead S, Bliss S, Baker PJ, Hunter CN (2017) Conserved residues in Ycf54 are required for protochlorophyllide formation in *Synechocystis* sp PCC 6803. Biochem J 474:667–681. https://doi.org/10.1042/BCJ20161002

Hong SJ, Kim H, Jang JH, Cho BK, Choi HK, Lee H, Lee CG (2014) Proteomic analysis of *Synechocystis* sp PCC 6803 responses to low-temperature and high light conditions. Biotech Bioprocess Eng 19:629–640. https://doi.org/10.1007/s12257-013-0563-2

Huang G, Xiao Y, Pi X, Zhao L, Zhu Q, Wang W, Kuang T, Han G, Sui SF, Shen JR (2021) Structural insights into a dimeric Psb27-photosystem II complex from a cyanobacterium *Thermosynechococcus vulcanus*. Proc Natl Acad Sci USA 118:e2018053118. https://doi.org/10.1073/pnas.2018053118

Huokko T, Ni T, Dykes GF, Simpson DM, Brownridge P, Conradi FD, Beynon RJ, Nixon PJ, Mullineaux CW, Zhang P, Liu LN (2021) Probing the biogenesis pathway and dynamics of thylakoid membranes. Nat Commun 12:1–14. https://doi.org/10.1038/s41467-021-23680-1

Islam MR, Aikawa S, Midorikawa T, Kashino Y, Satoh K, Koike H (2008) Slr 1923 of *Synechocysti*s sp PCC 6803 is essential for conversion of 3,8-divinyl(proto)chlorophyll(ide) to 3-monovinyl(proto)chlorophyll(ide). Plant Physiol 148:1068–1081. https://doi.org/10.1104/pp.108.123117

Ito H, Yokono M, Tanaka R, Tanaka A (2008) Identification of a novel vinyl reductase gene essential for the biosynthesis of monovinyl chlorophyll in *Synechocystis* sp. PCC6803. J Biol Chem 283:9002–9011. https://doi.org/10.1074/jbc.M708369200

Jablonsky J, Papacek S, Hagemann M (2016) Different strategies of metabolic regulation in cyanobacteria: from transcriptional to biochemical control. Sci Rep 6:33024. https://doi.org/10.1038/srep33024

Janasch M, Asplund-Samuelsson J, Steuer R, Hudson EP (2019) Kinetic modeling of the Calvin cycle identifies flux control and stable metabolomes in Synechocystis carbon fixation. J Exp Bot 70:973–983. https://doi.org/10.1093/jxb/ery382

Jordan P, Fromme P, Witt HT, Klukas O, Saenger W, Krausz N (2001) Three-dimensional structure of cyanobacterial photosystem I at 2.5 Å resolution. Nature 411:909–917. https://doi.org/10.1038/35082000

Kaneko T, Sato S, Kotani H, Tanaka A, Asamizu E, Nakamura Y, Miyajima N, Hirosawa M, Sugiura M, Sasamoto S, Kimura T, Hosouchi T, Matsuno A, Muraki A, Nakazaki N, Naruo K, Okumura S, Shimpo S, Takeuchi C, Wada T, Watanabe A, Yamada M, Yasuda M, Tabata S (1996) Sequence analysis of the genome of the unicellular cyanobacterium *Synechocystis* sp. strain PCC 6803. II. sequence determination of the entire genome and assignment of potential protein-coding regions. DNA Res 3:109–136. https://doi.org/10.1093/dnares/3.3.109

Karger GA, Reid JD, Hunter CN (2001) Characterization of the binding of deuteroporphyrin IX to the magnesium chelatase H subunit and spectroscopic properties of the complex. Biochemistry 40:9291–9299. https://doi.org/10.1021/bi010562a

Keren N, Aurora R, Pakrasi HB (2004) Critical roles of bacterioferritins in iron storage and proliferation of cyanobacteria. Plant Physiol 135:1666–1673. https://doi.org/10.1104/pp.104.042770

Kinney JN, Salmeen A, Cai F, Kerfeld CA (2012) Elucidating essential role of conserved carboxysomal protein CcmN reveals common feature of bacterial microcompartment assembly. J Biol Chem 287:17729–17736. https://doi.org/10.1074/jbc.M112.355305

Kirkpatrick DS, Gerber SA, Gygi SP (2005) The absolute quantification strategy: a general procedure for the quantification of proteins and post-translational modifications. Methods 35:265–273. https://doi.org/10.1016/j.ymeth.2004.08.018

Kiss É, Knoppová J, Aznar GP, Pilný J, Yu J, Halada P, Nixon PJ, Sobotka R, Komenda J (2019) A photosynthesis-specific rubredoxin-like protein is required for efficient association of the D1 and D2 proteins during the initial steps of photosystem II assembly. Plant Cell 31:2241–2258. https://doi.org/10.1105/tpc.19.00155

Klinkert B, Ossenbühl F, Sikorski M, Berry S, Eichacker L, Nickelsen J (2004) PratA, a periplasmic tetratricopeptide repeat protein involved in biogenesis of photosystem II in *Synechocystis* sp. PCC 6803. J Biol Chem 279:44639–44644. https://doi.org/10.1074/jbc.M405393200

Knoppová J, Sobotka R, Tichý M, Yu J, Konik P, Halada P, Nixon PJ, Komenda J (2014) Discovery of a chlorophyll binding protein complex involved in the early steps of photosystem II assembly in *Synechocystis*. Plant Cell 26:1200–1212. https://doi.org/10.1105/tpc.114.123919

Knoppová J, Sobotka R, Yu J, Bečková M, Pilný J, Trinugroho JP, Csefalvay L, Bína D, Nixon PJ, Komenda J (2022) Assembly of D1/D2 complexes of photosystem II: Binding of pigments and a network of auxiliary proteins. Plant Physiol 189:790–804. https://doi.org/10.1093/plphys/kiac045

Koebmann BJ, Westerhoff HV, Snoep JL, Nilsson D, Jensen PR (2002) The glycolytic flux in *Escherichia coli* is controlled by the demand for ATP. J Bact 184:3909–3916. https://doi.org/10.1128/JB.184.14.3909-3916.2002

Koksharova O, Schubert M, Shestakov S, Cerff R (1998) Genetic and biochemical evidence for distinct key functions of two highly divergent GAPDH genes in catabolic and anabolic carbon flow of the cyanobacterium *Synechocystis* sp. PCC 6803. Plant Mol Biol 36:183–194. https://doi.org/10.1023/a:1005925732743

Komenda J (2005) Autotrophic cells of the *Synechocystis* psbH deletion mutant are deficient in synthesis of CP47 and accumulate inactive PS II core complexes. Photosynthesis Res 85:161–167. https://doi.org/10.1007/s11120-005-1294-9

Komenda J, Lupínková L, Kopecký J (2002) Absence of the *psbH* gene product destabilizes photosystem II complex and bicarbonate binding on its acceptor side in *Synechocystis* PCC 6803. Eur J Biochem. https://doi.org/10.1046/j.0014-2956.2001.02693.x

Komenda J, Barker M, Kuviková S, De Vries R, Mullineaux CW, Tichý M, Nixon PJ (2006) The FtsH protease Slr0228 is important for quality control of photosystem II in the thylakoid membrane of *Synechocystis* sp. PCC 6803. J Biol Chem 281:1145–1151. https://doi.org/10.1074/jbc.M503852200

Komenda J, Knoppová J, Kopečná J, Sobotka R, Halada P, Yu J, Nickelsen J, Boehm M, Nixon PJ (2012) The Psb27 assembly factor binds to the CP43 complex of photosystem II in the cyanobacterium *Synechocystis* sp. PCC 6803. Plant Physiol 158:476–486. https://doi.org/10.1104/pp.111.184184

Konert MM, Wysocka A, Koník P, Sobotka R (2022) High-light-inducible proteins HliA and HliB: pigment binding and protein–protein interactions. Photosynth Res 26:1–6. https://doi.org/10.1007/s11120-022-00904-z

Kopečná J, Cabeza de Vaca I, Adams NBP, Davison PA, Brindley AA, Hunter CN, Guallar V, Sobotka R (2015) Porphyrin binding to Gun4 protein, facilitated by a flexible loop, controls metabolite flow through the chlorophyll biosynthetic pathway. J Biol Chem 290:28477–28488. https://doi.org/10.1074/jbc.M115.664987

Kramer DM, Avenson TJ, Edwards GE (2004) Dynamic flexibility in the light reactions of photosynthesis governed by both electron and proton transfer reactions. Trends Plant Sci 9:349–357. https://doi.org/10.1016/j.tplants.2004.05.001

Krey JF, Wilmarth PA, Shin JB, Klimek J, Sherman NE, Jeffery ED, Choi D, David LL, Barr-Gillespie PG (2014) Accurate label-free protein quantitation with high- and low-resolution mass spectrometers. J Proteome Res 13:1034–1044. https://doi.org/10.1021/pr401017h

Kroll D, Meierhoff K, Bechtold N, Kinoshita M, Westphal S, Vothknecht UC, Soll J, Westhoff P (2001) VIPP1, a nuclear gene of *Arabidopsis thaliana* essential for thylakoid membrane formation. Proc Natl Acad Sci USA 98:4238–4242. https://doi.org/10.1073/pnas.061500998

Krynická V, Tichý M, Krafl J, Yu J, Kaňa R, Boehm M, Nixon PJ, Komenda J (2014) Two essential FtsH proteases control the level of the Fur repressor during iron deficiency in the cyanobacterium *Synechocystis* sp. PCC 6803. Mol Microbiol 94:609–624. https://doi.org/10.1111/mmi.12782

Krynická V, Georg J, Jackson PJ, Dickman MJ, Hunter CN, Futschik ME, Hess WR, Komenda J (2019) Depletion of the FtsH1/3 proteolytic complex suppresses the nutrient stress response in the cyanobacterium *Synechocystis* sp strain PCC 6803. Plant Cell 31:2912–2928. https://doi.org/10.1105/tpc.19.00411

Kudva R, Denks K, Kuhn P, Vogt A, Müller M, Koch HG (2013) Protein translocation across the inner membrane of Gram-negative bacteria: the Sec and Tat dependent protein transport pathways. Res Microbiol 164:505–534. https://doi.org/10.1016/j.resmic.2013.03.016

Kwon J, Oh J, Park C, Cho K, Kim SI, Kim S, Lee S, Bhak J, Norling B, Choi JS (2010) Systematic cyanobacterial membrane proteome analysis by combining acid hydrolysis and digestive enzymes with nano-liquid chromatography–Fourier transform mass spectrometry. J Chromatogr A 1217:285–293. https://doi.org/10.1016/j.chroma.2009.11.045

Kwon JH, Bernát G, Wagner H, Rögner M, Rexroth S (2013) Reduced light-harvesting antenna: consequences on cyanobacterial metabolism and photosynthetic productivity. Algal Res 2:188–195. https://doi.org/10.1016/j.algal.2013.04.008

Lagarde D, Vermaas W (1999) The zeaxanthin biosynthesis enzyme beta-carotene hydroxylase is involved in myxoxanthophyll synthesis in *Synechocystis* sp. PCC 6803. FEBS Lett 454:247–251. https://doi.org/10.1016/s0014-5793(99)00817-0

Larkin RM, Alonso JM, Ecker JR, Chory J (2003) GUN4, a regulator of chlorophyll synthesis and intracellular signalling. Science 299:902–906. https://doi.org/10.1126/science.1079978

Laughlin TG, Savage DF, Davies KM (2020) Recent advances on the structure and function of NDH-1: The complex I of oxygenic photosynthesis. Biochim Biophys Acta Bioenerg 1861:148254. https://doi.org/10.1016/j.bbabio.2020.148254

Lea-Smith DJ, Bombelli P, Dennis JS, Scott SA, Smith AG, Howe CJ (2014) Phycobilisome-deficient strains of *Synechocystis* sp PCC 6803 have reduced size and require carbon-limiting conditions to exhibit enhanced productivity. Plant Physiol 165:705–714. https://doi.org/10.1104/pp.114.237206

Lea-Smith DJ, Bombelli P, Vasudevan R, Howe CJ (2016) Photosynthetic, respiratory and extracellular electron transport pathways in cyanobacteria. Biochim Biophys Acta Bioenerg 1857:247–255. https://doi.org/10.1016/j.bbabio.2015.10.007

Leister D (2012) How can the light reactions of photosynthesis be improved in plants? Front Plant Sci 3:199. https://doi.org/10.3389/fpls.2012.00199

Li F, Murillo C, Wurtzel ET (2007) Maize Y9 encodes a product essential for 15-*cis*-ζ-carotene isomerization. Plant Physiol 144:1181–1189. https://doi.org/10.1104/pp.107.098996

Li J, Zhou L, Wang H, Yan H et al (2015) A new sample preparation method for the absolute quantitation of a target proteome using ^{18}O labeling combined with multiple reaction monitoring mass spectrometry. Analyst 140:1281–1290. https://doi.org/10.1039/c4an02092h

Liang CW, Zhang XW, Tian L, Qin S (2008) Functional characterization of sll0659 from Synechocystis sp PCC 6803. Indian J Biochem Biophys 45:275–277

Lin Z, Ren Y, Shi Z, Zhang K, Yang H, Liu S, Hao P (2020) Evaluation and minimization of nonspecific tryptic cleavages in proteomic sample preparation. Rapid Commun Mass Spectrom 34:e8733. https://doi.org/10.1002/rcm.8733

Long BM, Badger MR, Whitney SM, Price GD (2007) Analysis of carboxysomes from *Synechococcus* PCC7942 reveals multiple Rubisco complexes with carboxysomal proteins CcmM and CcaA. J Biol Chem 282:29323–29335. https://doi.org/10.1074/jbc.M703896200

MacGregor-Chatwin C, Sener M, Barnett SFH, Hitchcock A, Barnhart-Dailey MC, Maghlaoui K, Barber J, Timlin JA, Schulten K, Hunter CN (2017) Lateral segregation of photosystem I in cyanobacterial thylakoids. Plant Cell 29:1119–1136. https://doi.org/10.1105/tpc.17.00071

MacLean B, Tomazela DM, Shulman N, Chambers M, Finney GL, Frewen B, Kern R, Tabb DL, Liebler DC, MacCoss MJ (2010) Skyline: an open source document editor for creating and analyzing targeted proteomics experiments. Bioinformatics 26:966–968. https://doi.org/10.1093/bioinformatics/btq054

Mahbub M, Hemm L, Yang Y, Kaur R, Carmen H, Engl C, Huokko T, Riediger M, Watanabe S, Liu L-N, Wilde A, Hess WR, Mullineaux CW (2020) mRNA localization, reaction centre biogenesis and Thylakoid membrane targeting in cyanobacteria. Nat Plants 6:1179–1191. https://doi.org/10.1038/s41477-020-00764-2

Malavath T, Caspy I, Netzer-El SY, Klaiman D, Nelson N (2018) Structure and function of wild-type and subunit-depleted photosystem I in *Synechocystis*. Biochim Biophys Acta Bioenerg 1859:645–654. https://doi.org/10.1016/j.bbabio.2018.02.002

Malmström J, Beck M, Schmidt A, Lange V, Deutsch EW, Aebersold R (2009) Proteome-wide cellular protein concentrations of the human pathogen *Leptospira interrogans*. Nature 460:762–765. https://doi.org/10.1038/nature08184

Malone LA, Qian P, Mayneord GE et al (2019) Cryo-EM structure of the spinach cytochrome b_6f complex at 3.6 Å resolution. Nature 575:535–539. https://doi.org/10.1038/s41586-019-1746-6

Malone LA, Proctor MS, Hitchcock A, Hunter CN, Johnson MP (2021) Cytochrome b_6f – Orchestrator of photosynthetic electron transfer. Biochim Biophys Acta Bioenerg 1862:148380. https://doi.org/10.1016/j.bbabio.2021.148380

Mann NH, Novac N, Mullineaux CW, Newman J, Bailey S, Robinson C (2000) Involvement of an FtsH homologue in the assembly of functional photosystem I in the cyanobacterium *Synechocystis* sp. PCC 6803. FEBS Lett 479:72–77. https://doi.org/10.1016/s0014-5793(00)01871-8

Maresca JA, Graham JE, Wu M, Eisen JA, Bryant DA (2007) Identification of a fourth family of lycopene cyclases in photosynthetic bacteria. Proc Natl Acad Sci USA 104:11784–11789. https://doi.org/10.1073/pnas.0702984104

Masamoto K, Wada H, Kaneko T, Takaichi S (2001) Identification of a gene required for cis-to-trans carotene isomerization in carotenogenesis of the cyanobacterium *Synechocystis* sp. PCC 6803. Plant Cell Physiol 42:1398–1402. https://doi.org/10.1093/pcp/pce167

McGurn LD, Moazami-Goudarzi M, White SA, Suwal T, Brar B, Tang JQ, Espie GS, Kimber MS (2016) The structure, kinetics and interactions of the β-carboxysomal β-carbonic anhydrase, CcaA. Biochem J 473:4559–4572. https://doi.org/10.1042/BCJ20160773

Meurer J, Plücken H, Kowallik KV, Westhoff P (1998) A nuclear-encoded protein of prokaryotic origin is essential for the stability of photosystem II in *Arabidopsis thaliana*. EMBO J 17:5286–5297. https://doi.org/10.1093/emboj/17.18.5286

Millán-Oropeza A, Blein-Nicolas M, Monnet V, Zivy M, Henry C (2022) Comparison of different label-free techniques for the semi-absolute quantification of protein abundance. Proteomes 10:2. https://doi.org/10.3390/proteomes10010002

Minamizaki K, Mizoguchi T, Goto T, Tamiaki H, Fujita Y (2008) Identification of two homologous genes, *chlAI* and *chlAII*, that are differentially involved in isocyclic ring formation of chlorophyll *a* in the cyanobacterium *Synechocystis* sp PCC 6803. J Biol Chem 283:2684–2692. https://doi.org/10.1074/jbc.M708954200

Moal G, Lagoutte B (2012) Photo-induced electron transfer from photosystem I to $NADP^+$: characterization and tentative simulation of the in vivo environment. Biochim Biophys Acta Bioenerg 1817:1635–1645. https://doi.org/10.1016/j.bbabio.2012.05.015

Muntel J, Fromion V, Goelzer A, Maaβ S, Mäder U, Büttner K, Hecker M, Becher D (2014) Comprehensive absolute quantification of the cytosolic proteome of Bacillus subtilis by data independent, parallel fragmentation in liquid chromatography/mass spectrometry (LC/MSE). Mol Cell Proteomics 13:1008–1019. https://doi.org/10.1074/mcp.M113.032631

Mustila H, Paananen P, Battchikova N, Santana-Sánchez A, Muth-Pawlak D, Hagemann M, Aro EM, Allahverdiyeva Y (2016) The flavodiiron protein Flv3 functions as a homo-oligomer during stress acclimation and is distinct from the Flv1/Flv3 hetero-oligomer specific to the O_2 photoreduction pathway. Plant Cell Physiol 57:1468–1483. https://doi.org/10.1093/pcp/pcw047

Muzzopappa F, Kirilovsky D (2020) Changing color for photoprotection: the orange carotenoid protein. Trends Plant Sci 25:92–104. https://doi.org/10.1016/j.tplants.2019.09.013

Naver H, Rochaix BE, JD, (2001) Functional studies of Ycf3: its role in assembly of photosystem I and interactions with some of its subunits. Plant Cell 13:2731–2745. https://doi.org/10.1105/tpc.010253

Nellaepalli S, Kim RG, Grossman AR, Takahashi Y (2021) Interplay of four auxiliary factors is required for the assembly of photosystem I reaction center subcomplex. Plant J 106:1075–1086. https://doi.org/10.1111/tpj.15220

Niedzwiedzki DM, Tronina T, Liu H, Staleva H, Komenda J, Sobotka R, Blankenship RE, Polívka T (2016) Carotenoid-induced non-photochemical quenching in the cyanobacterial chlorophyll synthase–HliC/D complex. Biochim Biophys Acta Bioenerg 1857:1430–1439. https://doi.org/10.1016/j.bbabio.2016.04.280

Nixon PJ, Barker M, Boehm M, de Vries R, Komenda J (2005) FtsH-mediated repair of the photosystem II complex in response to light stress. J Exp Bot 56:357–363. https://doi.org/10.1093/jxb/eri021

Ozawa SI, Nield J, Terao A, Stauber EJ, Hippler M, Koike H, Rochaix JD, Takahashi Y (2009) Biochemical and structural studies of the large Ycf4-photosystem I assembly complex of the green alga *Chlamydomonas reinhardtii*. Plant Cell 21:2424–2442. https://doi.org/10.1105/tpc.108.063313

Pan X, Cao D, Xie F, Xu F, Su X, Mi H, Zhang X, Li M (2020) Structural basis for electron transport mechanism of complex I-like photosynthetic NAD(P)H dehydrogenase. Nat Comm 11:610. https://doi.org/10.1038/s41467-020-14456-0

Pascual-Aznar G, Konert G, Bečková M, Kotabová E, Gardian Z, Knoppová J, Bučinská L, Kaňa R, Sobotka R, Komenda J (2021) Psb35 protein stabilizes the CP47 assembly module and associated high-light inducible proteins during the biogenesis of photosystem II in the cyanobacterium *Synechocystis* sp. PCC6803. Plant and Cell Physiol 62:178–190. https://doi.org/10.1093/pcp/pcaa148

Peng M, Taouatas N, Cappadona S, Van Breukelen B, Mohammed S, Scholten A, Heck AJ (2012) Protease bias in absolute protein quantitation. Nat Methods 9:524–525. https://doi.org/10.1038/nmeth.2031

Perez-Riverol Y, Csordas A, Bai J, Bernal-Llinares M, Hewapathirana S, Kundu DJ, Inuganti A, Griss J, Mayer G, Eisenacher M, Pérez E (2019) The PRIDE database and related tools and resources in 2019: improving support for quantification data. Nucleic Acids Res 47:D442–D450. https://doi.org/10.1093/nar/gky1106

Peter E, Salinas A, Wallner T, Jeske D, Dienst D, Wilde A, Grimm B (2009) Differential requirement of two homologous proteins encoded by *sll1214* and *sll1874* for the reaction of Mg proto-porphyrin monomethylester oxidative cyclase under aerobic and micro-oxic growth conditions. Biochim Biophys Acta Bioenerg 1787:1458–1467. https://doi.org/10.1016/j.bbabio.2009.06.006

Pisareva T, Kwon J, Oh J, Kim S, Ge C, Wieslander A, Choi JS, Norling B (2011) Model for membrane organization and protein sorting in the cyanobacterium *Synechocystis* sp PCC 6803 inferred from proteomics and multivariate sequence analyses. J Proteome Res 10:3617–3631. https://doi.org/10.1021/pr200268r

Pogoryelov D, Reichen C, Klyszejko AL, Brunisholz R, Muller DJ, Dimroth P, Meier T (2007) The oligomeric state of c rings from cyanobacterial F-ATP synthases varies from 13 to 15. J Bact 189:5895–5902. https://doi.org/10.1128/JB.00581-07

Porra RJ, Thompson WA, Kriedmann PE (1989) Determination of accurate extinction coefficients and simultaneous equations for assaying chlorophylls *a* and *b* extracted with four different solvents: verification of the concentration of chlorophyll standards by atomic absorption spectroscopy. Biochim Biophys Acta Bioenerg 975:384–394. https://doi.org/10.1016/S0005-2728(89)80347-0

Pratt JM, Simpson DM, Doherty MK, Rivers J, Gaskell SJ, Beynon RJ (2006) Multiplexed absolute quantification for proteomics using concatenated signature peptides encoded by QconCAT genes. Nat Protoc 1:1029–1043. https://doi.org/10.1038/nprot.2006.129

Proctor MS, Chidgey JW, Shukla MK, Jackson PJ, Sobotka R, Hunter CN, Hitchcock A (2018) Functional production of plant and algal chlorophyll synthases in cyanobacteria reveal a conserved interaction with the YidC/Alb3 membrane insertase. FEBS Lett 592:3062–3073. https://doi.org/10.1002/1873-3468.13222

Proctor MS, Pazderník M, Jackson PJ, Pilný J, Martin EC, Dickman MJ, Canniffe DP, Johnson MP, Hunter CN, Sobotka R, Hitchcock A (2020) Xanthophyll carotenoids stabilise the association of cyanobacterial chlorophyll synthase with the LHC-like protein HliD. Biochem J 477:4021–4036. https://doi.org/10.1042/BCJ20200561

Proctor MS, Sutherland GA, Canniffe DP, Hitchcock A (2022a) The terminal enzymes of (bacterio)chlorophyll biosynthesis. R Soc Open Sci 9:211903. https://doi.org/10.1098/rsos.211903

Proctor MS, Malone LA, Farmer DA et al (2022b) Cryo-EM structures of the *Synechocystis* sp. PCC 6803 cytochrome b6f complex with and without the regulatory PetP subunit. Biochem J 479:1487–1503. https://doi.org/10.1042/BCJ20220124

Proctor MS, Morey-Burrows FS, Canniffe DP, Martin EC, Swainsbury DJK, Johnson MP, Hunter CN, Sutherland GA, Hitchcock A (2022c) Zeta-carotene isomerase (Z-ISO) is required for light-independent carotenoid biosynthesis in the cyanobacterium Synechocystis sp PCC 6803. Microorganisms 10:1730

Qian P, Papiz MZ, Jackson PJ, Brindley AA, Ng IW, Olsen JD, Dickman MJ, Bullough PA, Hunter CN (2013) Three-dimensional structure of the *Rhodobacter sphaeroides* RC-LH1-PufX complex: dimerization and quinone channels promoted by PufX. Biochemistry 52:7575–7585. https://doi.org/10.1021/bi4011946

Rae BD, Long BM, Badger MR, Price GD (2012) Structural determinants of the outer shell of β-carboxysomes in *Synechococcus elongatus* PCC 7942: roles for Ccm K2, K3–K4, CcmO, and CcmL. PLoS ONE 7:e43871. https://doi.org/10.1371/journal.pone.0043871

Rahimzadeh-Karvansara P, Pascual-Aznar G, Bečková M, Komenda J (2022) Psb34 protein modulates binding of high-light-inducible proteins to CP47-containing photosystem II assembly intermediates in the cyanobacterium *Synechocystis* sp. PCC 6803. Photosynth Res 13:1–4. https://doi.org/10.1007/s11120-022-00908-9

Rast A, Rengstl B, Heinz S, Klingl A, Nickelsen J (2016) The role of Slr0151, a tetratricopeptide repeat protein from *Synechocystis*
sp PCC 6803, during photosystem II assembly and repair. Front Plant Sci 7:605. https://doi.org/10.3389/fpls.2016.00605

Rast A, Schaffer M, Albert S, Wan W, Pfeffer S, Beck F, Plitzko JM, Nickelsen J, Engel BD (2019) Biogenic regions of cyanobacterial thylakoids form contact sites with the plasma membrane. Nat Plants 5:436–446. https://doi.org/10.1038/s41477-019-0399-7

Reid JD, Hunter CN (2004) Magnesium-dependent ATPase activity and cooperativity of magnesium chelatase from *Synechocystis* sp PCC 6803. J Biol Chem 279:26893–26899. https://doi.org/10.1074/jbc.M400958200

Reid JD, Siebert CA, Bullough PA, Hunter CN (2003) The ATPase activity of the ChlI subunit of magnesium chelatase and formation of a heptameric AAA+ ring. Biochemistry 42:6912–6920. https://doi.org/10.1021/bi034082q

Reinbothe C, El Bakkouri M, Buhr F, Muraki N, Nomata J, Kurisu G, Fujita Y, Reinbothe S (2010) Chlorophyll biosynthesis: spotlight on protochlorophyllide reduction. Trends Plant Sci 15:614–624. https://doi.org/10.1016/j.tplants.2010.07.002

Reinhold L, Kosloff R, Kaplan A (1991) A model for inorganic carbon fluxes and photosynthesis in cyanobacterial carboxysomes. Can J Bot 69:984–988. https://doi.org/10.1139/b91-12

Ren D, Pipes GD, Liu D, Shih LY, Nichols AC, Treuheit MJ, Brems DN, Bondarenko PV (2009) An improved trypsin digestion method minimizes digestion-induced modifications on proteins. Anal Biochem 392:12–21. https://doi.org/10.1016/j.ab.2009.05.018

Rengstl B, Knoppová J, Komenda J, Nickelsen J (2013) Characterization of a *Synechocystis* double mutant lacking the photosystem II assembly factors YCF48 and Sll0933. Planta 237:471–480. https://doi.org/10.1007/s00425-012-1720-0

Rexroth S, Rexroth D, Veit S, Plohnke N, Cormann KU, Nowaczyk MM, Rögner M (2014) Functional characterization of the small regulatory subunit PetP from the cytochrome b_6f complex in *Thermosynechococcus elongatus*. Plant Cell 26:3435–3448. https://doi.org/10.1105/tpc.114.125930

Rippka R, Deruelles J, Waterbury J, Herdman M, Stanier R (1979) Generic assignments, strain histories and properties of pure cultures of cyanobacteria. Microbiology 111:1–61. https://doi.org/10.1099/00221287-111-1-1

Rodgers AJW, Wilce MCJ (2000) Structure of the γ–ε complex of ATP synthase. Nat Struct Biol 7:1051–1054. https://doi.org/10.1038/80975

Rousseaux CS, Gregg WW (2014) Interannual variation in phytoplankton primary production at a global scale. Remote Sens 6:1–19. https://doi.org/10.3390/rs6010001

Rzeznicka K, Walker CJ, Westergren T, Kannangara CG, von Wettstein D, Merchant S, Gough SP, Hansson M (2005) Xantha-l encodes a membrane subunit of the aerobic Mg-protoporphyrin IX monomethyl ester cyclase involved in chlorophyll biosynthesis. Proc Natl Acad Sci USA 102:5886–5891. https://doi.org/10.1073/pnas.0501784102

Saunée NA, Williams SR, Bryant DA, Schluchter WM (2008) Biogenesis of Phycobiliproteins: II. CpcS-I and CpcU comprise the heterodimeric bilin lyase that attaches phycocyanobilin to cys-82 of beta-phycocyanin and cys-81 of allophycocyanin subunits in *Synechococcus* sp. PCC 7002. J Biol Chem 283:7513–7522. https://doi.org/10.1074/jbc.M708165200

Scheer H, Zhao KH (2008) Biliprotein maturation: the chromophore attachment. Mol Microbiol 68:263–276. https://doi.org/10.1111/j.1365-2958.2008.06160.x

Schluchter WM, Glazer AN (1997) Characterization of cyanobacterial biliverdin reductase. conversion of biliverdin to bilirubin is important for normal phycobiliprotein biosynthesis. J Biol Chem 272:13562–13569. https://doi.org/10.1074/jbc.272.21.13562

Schneider D, Volkmer T, Rögner M (2007) PetG and PetN, but not PetL, are essential subunits of the cytochrome b_6f complex

from *Synechocystis* PCC 6803. Res Microbiol 158:45–50. https://doi.org/10.1016/j.resmic.2006.10.002

Schottkowski M, Ratke J, Oster U, Nowaczyk M, Nickelsen J (2009) Pitt, a novel tetratricopeptide repeat protein involved in light-dependent chlorophyll biosynthesis and thylakoid membrane biogenesis in Synechocystis sp. PCC 6803. Mol Plant 2:1289–1297. https://doi.org/10.1093/mp/ssp075

Schöttler MA, Albus CA, Bock R (2011) Photosystem I: its biogenesis and function in higher plants. J Plant Physiol 168:1452–1461. https://doi.org/10.1016/j.jplph.2010.12.009

Schöttler MA, Tóth SZ, Boulouis A, Kahlau S (2015) Photosynthetic complex stoichiometry dynamics in higher plants: biogenesis, function, and turnover of ATP synthase and the cytochrome b 6 f complex. J Exp Bot 66:2373–2400. https://doi.org/10.1093/jxb/eru495

Schuller JM, Birrell JA, Tanaka H et al (2019) Structural adaptations of photosynthetic complex I enable ferredoxin-dependent electron transfer. Science 363:257–260. https://doi.org/10.1126/science.aau3613

Schwanhäusser B, Busse D, Li N, Dittmar G, Schuchhardt J, Wolf J, Chen W, Selbach M (2011) Global quantification of mammalian gene expression control. Nature 473:337–342. https://doi.org/10.1038/nature10098

Scott KB, Turko IV, Phinney KW (2015) Quantitative performance of internal standard platforms for absolute protein quantification using multiple reaction monitoring-mass spectrometry. Anal Chem 87:4429–4435. https://doi.org/10.1021/acs.analchem.5b00331

Sengupta A, Pakrasi HB, Wangikar PP (2018) Recent advances in synthetic biology of cyanobacteria. Appl Microbiol Biotechnol 102:5457–5471. https://doi.org/10.1007/s00253-018-9046-x

Shen G, Saunée NA, Williams SR, Gallo EF, Schluchter WM, Bryant DA (2006) Identification and characterization of a new class of bilin lyase: the cpcT gene encodes a blin lyase responsible for attachment of phycocyanobilin to Cys-153 on the β-subunit of phycocyanin in *Synechococcus* sp. PCC 7002. J Biol Chem 281:17768–17778. https://doi.org/10.1074/jbc.M602563200

Shepherd M, Hunter CN (2004) Transient kinetics of the reaction catalysed by magnesium protoporphyrin IX methyltransferase. Biochem J 382:1009–1013. https://doi.org/10.1042/BJ20040661

Shukla MK, Llansola-Portoles MJ, Tichý M, Pascal AA, Robert B, Sobotka R (2018) Binding of pigments to the cyanobacterial high-light-inducible protein HliC. Photosynth Res 137:29–39. https://doi.org/10.1007/s11120-017-0475-7

Silva P, Thompson E, Bailey S, Kruse O, Mullineaux CW, Robinson C, Mann NH, Nixon PJ (2003) FtsH is involved in the early stages of repair of photosystem II in *Synechocystis* sp PCC 6803. Plant Cell 15:2152–2164. https://doi.org/10.1105/tpc.012609

Silva JC, Gorenstein MV, Li GZ, Vissers JP, Geromanos SJ (2006) Absolute quantification of proteins by LCMSE: a virtue of parallel MS acquisition. Mol Cell Proteomics 5:144–156. https://doi.org/10.1074/mcp.M500230-MCP200

Singh S, Springer M, Steen J, Kirschner MW, Steen H (2009) FLEXIQuant: a novel tool for the absolute quantification of proteins, and the simultaneous identification and quantification of potentially modified peptides. J Proteome Res 8:2201–2210. https://doi.org/10.1021/pr800654s

Sirijovski N, Lundqvist J, Rosenback M, Elmlund H, Al-Karadaghi S, Willows RD, Hansson M (2008) Substrate-binding model of the chlorophyll biosynthetic magnesium chelatase BchH subunit. J Biol Chem 283:11652–11660. https://doi.org/10.1074/jbc.M709172200

Soll J, Schultz G, Rüdiger W, Benz J (1983) Hydrogenation of geranylgeraniol: two pathways exist in spinach chloroplasts. Plant Physiol 71:849–854. https://doi.org/10.1104/pp.71.4.849

Sozer O, Komenda J, Ughy B, Domonkos I, Laczko-Dobos H, Malec P et al (2010) Involvement of carotenoids in the synthesis and assembly of protein subunits of photosynthetic reaction centers of *Synechocystis* sp. PCC 6803. Plant Cell Physiol 51:823–835. https://doi.org/10.1093/pcp/pcq031

Staleva H, Komenda J, Shukla MK, Šlouf V, Kaňa R, Polívka T, Sobotka R (2015) Mechanism of photoprotection in the cyanobacterial ancestor of plant antenna proteins. Nat Chem Biol 11:287–291. https://doi.org/10.1038/nchembio.1755

Stengel A, Gügel IL, Hilger D, Rengstl B, Jung H, Nickelsen J (2012) Initial steps of photosystem II *de novo* assembly and preloading with manganese take place in biogenesis centers in *Synechocystis*. Plant Cell 24:660–675. https://doi.org/10.1105/tpc.111.093914

Suga M, Akita F, Hirata K et al (2015) Native structure of photosystem II at 1.95 Å resolution viewed by femtosecond X-ray pulses. Nature 517:99–103. https://doi.org/10.1038/nature13991

Summerfield TC, Toepel J, Sherman LA (2008) Low-oxygen induction of normally cryptic psbA genes in cyanobacteria. Biochemistry 47:12939–12941. https://doi.org/10.1021/bi8018916

Tanaka R, Tanaka A (2007) Tetrapyrrole biosynthesis in higher plants. Annu Rev Plant Biol 58:321–346. https://doi.org/10.1146/annurev.arplant.57.032905.105448

Tanaka S, Kerfeld CA, Sawaya MR, Cai F, Heinhorst S, Cannon GC, Yeates TO (2008) Atomic-level models of the bacterial carboxysome shell. Science 319:1083–1086. https://doi.org/10.1126/science.1151458

Tang J, Fu J, Wang Y et al (2019) Simultaneous improvement in the precision, accuracy, and robustness of label-free proteome quantification by optimizing data manipulation chains. Mol Cell Proteomics 18:1683–1699. https://doi.org/10.1074/mcp.RA118.001169

Thomas JC, Ughy B, Lagoutte B, Ajlani G (2006) A second isoform of the ferredoxin: NADP oxidoreductase generated by an in-frame initiation of translation. Proc Natl Acad Sci 103:18368–18373. https://doi.org/10.1073/pnas.0607718103

Tichý M, Bečková M, Kopečná J, Noda J, Sobotka R, Komenda J (2016) Strain of *Synechocystis* PCC 6803 with aberrant assembly of photosystem II contains tandem duplication of a large chromosomal region. Front Plant Sci 7:648. https://doi.org/10.3389/fpls.2016.00648

Tokumaru Y, Uebayashi K, Toyoshima M, Osanai T, Matsuda F, Shimizu H (2018) Comparative targeted proteomics of the central metabolism and photosystems in SigE mutant strains of *Synechocystis* sp PCC 6803. Molecules 23:1051. https://doi.org/10.3390/molecules23051051

Tottey S, Block MA, Allen M, Westergren T, Albrieux C, Scheller HV, Merchant S, Jensen PE (2003) Arabidopsis CHL27, located in both envelope and thylakoid membranes, is required for the synthesis of protochlorophyllide. Proc Natl Acad Sci USA 100:16119–16124. https://doi.org/10.1073/pnas.2136793100

Touloupakis E, Cicchi B, Torzillo G (2015) A bioenergetic assessment of photosynthetic growth of *Synechocystis* sp PCC 6803 in continuous cultures. Biotechnol Biofuels 8:1–11. https://doi.org/10.1186/s13068-015-0319-7

Tsunoyama Y, Bernát G, Dyczmons NG, Schneider D, Rögner M (2009) Multiple Rieske proteins enable short- and long-term light adaptation of *Synechocystis* sp PCC 6803. J Biol Chem 284:27875–27883. https://doi.org/10.1074/jbc.M109.011189

Tyanova S, Temu T, Sinitcyn P (2016) The Perseus computational platform for comprehensive analysis of (prote)omics data. Nat Methods 13:731–740. https://doi.org/10.1038/nmeth.3901

Ullah H, Nagelkerken I, Goldenberg SU, Fordham DA (2018) Climate change could drive marine food web collapse through altered trophic flows and cyanobacterial proliferation. PLOS Biol 16:e2003446. https://doi.org/10.1371/journal.pbio.2003446

Umena Y, Kawakami K, Shen JR, Kamiya N (2011) Crystal structure of oxygen-evolving photosystem II at a resolution of 1.9 Å. Nature 473:55–60. https://doi.org/10.1038/nature09913

Urbanus ML, Fröderberg L, Drew D, Björk P, de Gier JW, Brunner J, Oudega B, Luirink J (2002) Targetini insertion and localization of *Escherichia coli* YidC. J Biol Chem 277(15):12718–12723. https://doi.org/10.1074/jbc.M200311200

Veit S, Takeda K, Tsunoyama Y, Baymann F, Nevo R, Reich Z, Rögner M, Miki K, Rexroth S (2016a) Structural and functional characterisation of the cyanobacterial PetC3 Rieske protein family. Biochim Biophys Acta Bioenerg 1857:1879–1891. https://doi.org/10.1016/j.bbabio.2016.09.007

Veit S, Nagadoi A, Rögner M, Rexroth S, Stoll R, Ikegami T (2016b) The cyanobacterial cytochrome b_6f subunit PetP adopts an SH3 fold in solution. Biochim Biophys Acta Bioenerg 1857:705–714. https://doi.org/10.1016/j.bbabio.2016b.03.023

Venable JD, Dong MQ, Wohlschlegel J, Dillin A, Yates JR (2004) Automated approach for quantitative analysis of complex peptide mixtures from tandem mass spectra. Nat Methods 1:39–45. https://doi.org/10.1038/nmeth705

Vermaas WFJ (1994) Molecular–genetic approaches to study photosynthetic and respiratory electron transport in thylakoids from cyanobacteria. Biochim Biophys Acta Bioenerg 1187:181–186. https://doi.org/10.1016/0005-2728(94)90107-4

Vignais PM, Billoud B (2007) Occurrence, classification, and biological function of hydrogenases: an overview. Chem Rev 107:4206–4272. https://doi.org/10.1021/cr050196r

Viney J, Davison PA, Hunter CN, Reid JD (2007) Direct measurement of metal-ion chelation in the active site of the AAA+ ATPase magnesium chelatase. Biochemistry 46:12788–12794. https://doi.org/10.1021/bi701515y

Wilde A, Härtel H, Hübschmann T, Hoffmann P, Shestakov SV, Börner T (1995) Inactivation of a *Synechocystis* sp strain PCC 6803 gene with homology to conserved chloroplast open reading frame 184 increases the photosystem II-to-photosystem I ratio. Plant Cell 7:649–658. https://doi.org/10.1105/tpc.7.5.649

Wilde A, Lünser K, Ossenbühl F, Nickelsen J, Börner T (2001) Characterization of the cyanobacterial ycf37: mutation decreases the photosystem I content. Biochem J 357:211–216. https://doi.org/10.1042/bj3570211

Wiśniewski JR, Rakus D (2014) Multi-enzyme digestion FASP and the 'Total Protein Approach'-based absolute quantification of the *Escherichia coli* proteome. J Proteomics 109:322–331. https://doi.org/10.1016/j.jprot.2014.07.012

Xiong W, Shen G, Bryant DA (2017) *Synechocystis* sp. PCC 6803 CruA (sll0147) encodes lycopene cyclase and requires bound chlorophyll a for activity. Photosynth Res 131:267–280. https://doi.org/10.1007/s11120-016-0316-0

Xu C, Wang B, Yang L, Zhongming HuL, Yi L, Wang Y, Chen S, Emili A, Wan C (2021) Global landscape of native protein complexes in *Synechocystis* sp PCC 6803. Genomics Proteomics Bioinform. https://doi.org/10.1016/j.gpb.2020.06.020

Yamazaki S, Nomata J, Fujita Y (2006) Differential operation of dual protochlorophyllide reductases for chlorophyll biosynthesis in response to environmental oxygen levels in the cyanobacterium *Leptolyngbya boryana*. Plant Physiol 142:911–922. https://doi.org/10.1104/pp.106.086090

Yang H, Liao L, Bo T, Zhao L, Sun X, Lu X, Norling B, Huang F (2014) Slr0151 in *Synechocystis* sp. PCC 6803 is required for efficient repair of photosystem II under high-light condition. J Int Plant Biol 56:1136–1150. https://doi.org/10.1111/jipb.12275

Yeates TO, Thompson MC, Bobik TA (2011) The protein shells of bacterial microcompartment organelles. Curr Opin Struct Biol 21:223–231

Yilmaz M, Kang I, Beale SI (2010) Heme oxygenase 2 of the cyanobacterium *Synechocystis* sp. PCC 6803 is induced under a microaerobic atmosphere and is required for microaerobic growth at high light intensity. Photosynth Res 103:47–59. https://doi.org/10.1007/s11120-009-9506-3

Yoon HS, Hackett JD, Ciniglia C, Pinto G, Bhattacharya D (2004) A molecular timeline for the origin of photosynthetic eukaryotes. Mol Biol Evol 21:809–818. https://doi.org/10.1093/molbev/msh075

Yu J, Smart LB, Jung YS, Golbeck J, McIntosh L (1995) Absence of PsaC subunit allows assembly of photosystem I core but prevents the binding of PsaD and PsaE in *Synechocystis* sp. PCC6803. Plant Mol Biol 29:331–342. https://doi.org/10.1007/BF00043656

Yu J, Knoppová J, Michoux F et al (2018) Ycf48 involved in the biogenesis of the oxygen-evolving photosystem II complex is a seven-bladed beta-propeller protein. Proc Natl Acad Sci 115:E7824–E7833. https://doi.org/10.1073/pnas.1800609115

Zabret J, Bohn S, Schuller SK et al (2021) Structural insights into photosystem II assembly. Nat Plants 7:524–538. https://doi.org/10.1038/s41477-021-00895-0

Zavřel T, Očenášová P, Červený J (2017) Phenotypic characterization of *Synechocystis* sp PCC 6803 substrains reveals differences in sensitivity to abiotic stress. PLoS ONE 12:e0189130. https://doi.org/10.1371/journal.pone.0189130

Zhang S, Shen G, Li Z, Golbeck JH, Bryant DA (2014) Vipp1 is essential for the biogenesis of photosystem I but not thylakoid membranes in *Synechococcus* sp. PCC 7002. J Biol Chem 289:15904–15914. https://doi.org/10.1074/jbc.M114.555631

Zhang S, Godwin AR, Taylor A, Hardman SJ, Jowitt TA, Johannissen LO, Hay S, Baldock C, Heyes DJ, Scrutton NS (2021) Dual role of the active site 'lid' regions of protochlorophyllide oxidoreductase in photocatalysis and plant development. FEBS J 288:175–189. https://doi.org/10.1111/febs.15542

Zhao KH, Su P, Tu JM et al (2007) Phycobilin:cysteine-84 biliprotein lyase, a near-universal lyase for cysteine-84-binding sites in cyanobacterial phycobiliproteins. Proc Natl Acad Sci USA 104:14300–14305. https://doi.org/10.1073/pnas.0706209104

Zhao LS, Huokko T, Wilson S et al (2020) Structural variability, coordination and adaptation of a native photosynthetic machinery. Nat Plants 6:869–882. https://doi.org/10.1038/s41477-020-0694-3